UCRL-ID-128733

A Time-Dependent Buoyant Puff Model for Explosive Sources

E. J. Kansa

September 1, 1997

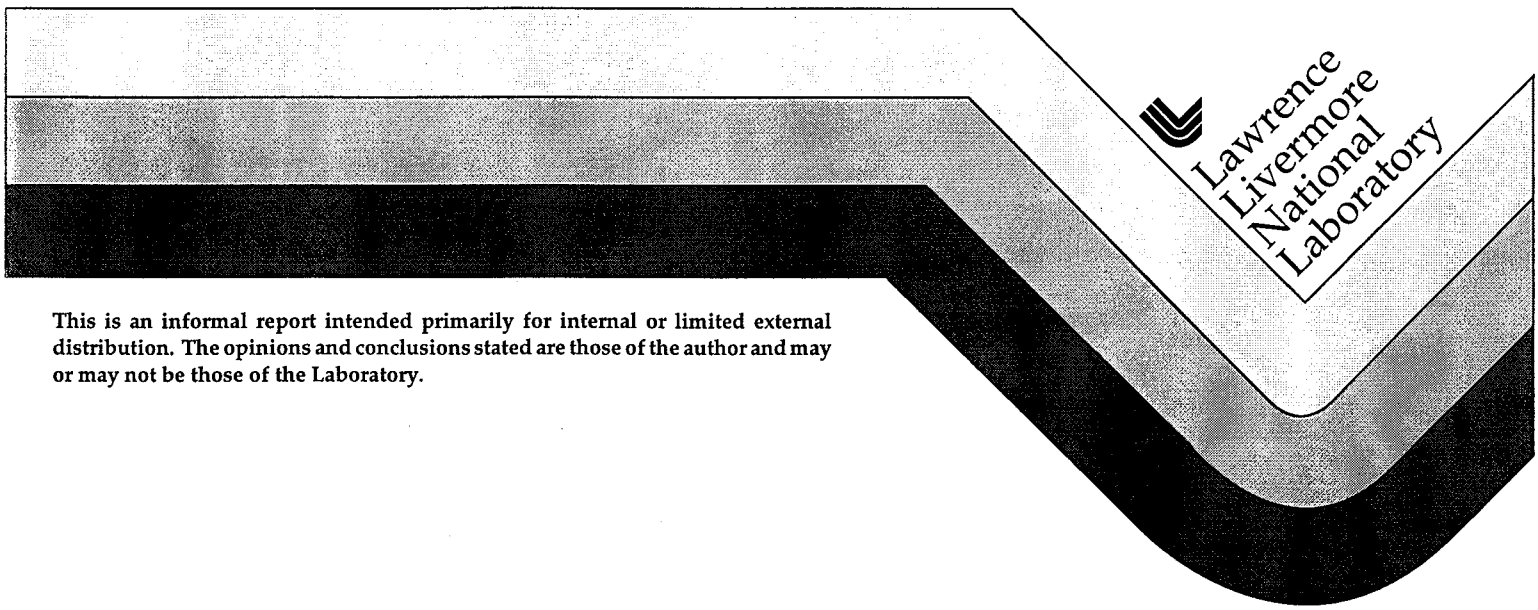

A TIME-DEPENDENT BUOYANT PUFF MODEL FOR EXPLOSIVE SOURCES

Edward J. Kansa
L-103
Lawrence Livermore National Laboratory
Livermore, CA 94551-9900

September, 1997

TABLE OF CONTENTS

A TIME-DEPENDENT BUOYANT PUFF MODEL FOR EXPLOSIVE SOURCES

Edward J. Kansa
L-103
Lawrence Livermore National Laboratory
Livermore, CA 94551-9900

Abstract

Several models exist to predict the time dependent behavior of buoyant puffs that result from explosions. This paper presents a new model that is derived from the strong conservative form of the conservation partial differential equations that are integrated over space to yield a coupled system of time dependent nonlinear ordinary differential equations. This model permits the cloud to evolve from an initial spherical shape into an ellipsoidal shape. It ignores the Boussinesq approximation, and treats the turbulence that is generated by the puff itself and the ambient atmospheric turbulence as separate mechanisms in determining the puff history. The puff cloud rise history was found to depend not only on the mass and initial temperature of the explosion, but also upon the stability conditions of the ambient atmosphere. This model was calibrated by comparison with the Roller Coaster experiments.

1.0 Introduction

A two-dimensional or fully three-dimensional time dependent model of buoyant puff rise is impractical in the context of the real time LLNL-National Atmospheric Response Advisory Capability. Consequently, the present approach deals with only volume-averaged quantities that give the time-dependent response of buoyant puffs arising from explosions. This approach reduces the model to a set of coupled, nonlinear ordinary differential equations that can be integrated very rapidly. A simplified puff-atmospheric turbulence model that is dependent upon the Richardson number is developed. This explosive source model is subsequently used to initialize the source in a particle dispersion model.

2.0 Approach

The three-dimensional Navier-Stokes equations in the strong conservative form is the starting point of the derivation of this work. Recognizing that the puff cloud arising from an explosion is a discontinuity, the Navier-Stokes equations are integrated over space to yield a set of coupled nonlinear time dependent ordinary differential equations (ODEs) in terms of the jumps in the dependent variables across the discontinuity. The flow variables are assumed to be a sum of mean and fluctuating flow quantities. The mean flow is assumed to be responsible for entrainment while the fluctuating turbulent quantities arise from the ambient atmosphere and the hot puff itself. The atmospheric stability was found to play a major role in determining the rise history of an explosion.

2.1. Basic Nature of Explosion Clouds

Baker et al.(1983) define an explosion as a rapid exothermic chemical reaction that produces an

overpressure that can be heard. Explosions can be due to either high explosives (e.g, TNT), propellants, or hydrocarbon fires. High explosives have very short reaction times that produce very hot gases (T_{expl}~5,000 K) whereas hydrocarbon explosions are much cooler (T_{expl}~ 1,350 K) and whose reaction time is much longer. They present empirical relations for a fireball radius and duration in terms of the mass equivalent of TNT, M, as

$$R^* = 1.93\, M^{0.32} / (T_{expl}/3600)^{1/3} \quad (1)$$

$$t^* = 0.299 M^{0.32} / (T_{expl}/3600)^{10/3} \quad (2)$$

While the chemical reaction is proceeding, it is convenient to approximate the spherical volume of radius, R*, see Eq.(1), with a uniform burn temperature, T_{expl}. The radius grows at the rate, R*/t* until the time, t^* is reached and the chemical reactions cease. The hot sphere starts to rise immediately after its temperature is above the ambient temperature. In addition, it is well known that turbulence is enhanced in gases lighter than air. After the time, t*, all the chemical reactions in the puff are completed. The hot gases rise, expand, entrains and turbulently mix the cool atmospheric air, distort in shape, and eventually rise to a final height in equilibrium with the atmosphere. The equilibrium height to which the puff rises is strongly dependent upon the atmospheric stability condition and will discussed later.

2.2. Basic Model Formulation

After the puff has entrained a sufficient amount of air, and, the puff stops rising at a height, H.

Asymptotically,

$$w_p(H) \rightarrow 0, \quad (3.a)$$

$$u_p(H) \rightarrow u_a(H) \quad (3.b)$$

$$\rho_p(H) \rightarrow \rho_a(H) \quad (3.c)$$

$$T_p(H) \rightarrow T_a(H) \quad (3.d)$$

where w_p is the vertical component of the puff velocity, u_p is the lateral component of the puff velocity, ρ_p is the density of the puff gases, and T_p is the temperature of the puff gases.

The puff turbulent eddy viscosity and thermal conductivity approach zero, and only the atmospheric turbulence remains,

$$\mu_p(H) \rightarrow 0, \quad (3.e)$$

$$\kappa_p(H) \rightarrow 0. \quad (3.f)$$

where μ_p and κ_p are the puff-atmospheric turbulent eddy viscosity and thermal conductivities, respectively.

The starting point for deriving the buoyant puff model is the strong conservative form of the Navier-Stokes equations for conservation of mass, momentum, and total energy. The motivation

for using this form of the conservation equations is that the volume integration simplifies the results by using the Gauss divergence theorem. These conservation equations are written in terms of mean and fluctuating variables. The mean flow is responsible for "entrainment" whereas the fluctuating flow is responsible for turbulent mixing and dissipation. To derive the appropriate ordinary differential equations, it is assumed that the dependent variables for mass, momentum, and energy are expanded in terms of the mean values and the turbulent fluctuations, i.e., $\rho = \bar{\rho} + \rho''$, $u = \bar{u} + u''$, etc. Doublet and triplet terms of the fluctuating variables are considered. These terms assume a dry atmosphere in which the effects of water vapor are small. (Note that water vapor can be included as an additional conservation equation if consider significant in a particular application.).

$$\partial\rho/\partial t + \nabla\bullet(\rho\mathbf{u}) = 0 \tag{4}$$

$$\partial(\rho\mathbf{u})/\partial t + \nabla\bullet(PI + \rho\mathbf{uu}) = (\rho_a - \rho_p)\, g\, \mathbf{k} \tag{5}$$

$$\partial\rho E/\partial t + \nabla\bullet((\rho E+p)\mathbf{u}) = \varepsilon\sigma(T_p^4 - T_a^4) + (\rho_a - \rho_p)g(\mathbf{k}\bullet\mathbf{w}) \tag{6}$$

where all gases are assumed to be ideal,

$$P = (R/M)\rho T = \Re\rho T. \tag{7}$$

$$c_p - c_v = \Re \tag{8}$$

$$c_p/c_v = \gamma. \tag{9}$$

where $\mathbf{k}$ is a unit vector in the vertical (z) direction, g is the acceleration of gravity, $\Re$ is the ideal gas constant divided by the molecular weight of air, c_p and c_v are the heat capacities of air at constant pressure and constant volume, respectively, γ is the ratio of heat capacity at constant pressure to constant volume, σ is the Stefan-Boltzman constant, ε is the emissivity of the dry atmosphere, and $\mathbf{I}$ is the identity tensor. P, ρ, and T refer to ideal gas pressure, density and temperature, respectively, and $\mathbf{u}$ is a vector representing the fluid velocity.

The total energy density is related to the pressure and temperature by the following relations:

$$\rho E = P/(\gamma - 1) + \rho\, \mathbf{u}\bullet\mathbf{u}/2, \tag{10}$$

and

$$T = (E - \mathbf{u}\bullet\mathbf{u}/2)/c_v. \tag{11}$$

The boundary between the ambient atmosphere and the hot plume is assumed to be a "discontinuity" over which the temperature, density, and velocities vary rapidly. The rapid chemical reaction produces an overpressure in the hot puff that propagates this boundary into the ambient atmosphere both laterally and vertically. Even though the chemical reactions are completed, the hot gas still possesses sufficient radial momentum to continue expanding; however, this rate of expansion decays due to spherical divergence. In actuality, the expansion rate will decay even faster because of turbulence. A convenient and reasonable assumption is

that the pressure inside the puff is equal to that of the atmosphere at the height, z.

$$P_p(z) = P_a(z). \tag{12}$$

The vertical momentum component is initially zero, but the buoyant hot gas induces a vertical component of momentum upon the existing radial momentum. Thus, the spherical explosion will eventually distort into an idealized elongated ellipsoidal shape.

2.3. The explosive puff as an ensemble of simple geometric shapes

Many of the previous attempts at modeling puff rise constrained the puff to be spherical throughout the entire rise. The puff appears to be more complicated with the initial spherical cloud evolving into a mushroom-shaped cloud. The present model assumes that the mushroom cap is composed to two half-ellipsoids with a common radius, r, in the horizontal plane. The stem is assumed to resemble a cylinder. The upper portion of the cap is a half-ellipsoid of height above the center, z, h^+, and the lower portion is an ellipsoid of height, h^-, below the center, z.

The rationale behind considering the cap to be composed of two half ellipsoids can be explained as follows. The center of the cap rises at the velocity, w_p. Initially, the spherical puff is expanding at a speed, s. By vector addition, the interface at the top and bottom of the puff will experience different net velocities, and gradually, h^+ and, h^{--} will be distinct

The notation, $h^{\pm}$, refers to either h^+ or h^-. The equation for an ellipsoid is:

$$(x^2+ y^2)/r^2 + z^2/(h^{\pm})^2 = 1. \tag{13}$$

Note, if $h^+ = h^- = r$, then this ellipsoid degenerates to a sphere: if $h^{\pm} < r$, the puff is flattened (oblate ellipsoid) whereas if $h^{\pm} > r$, the puff is elongated or a (prolate ellipsoid).

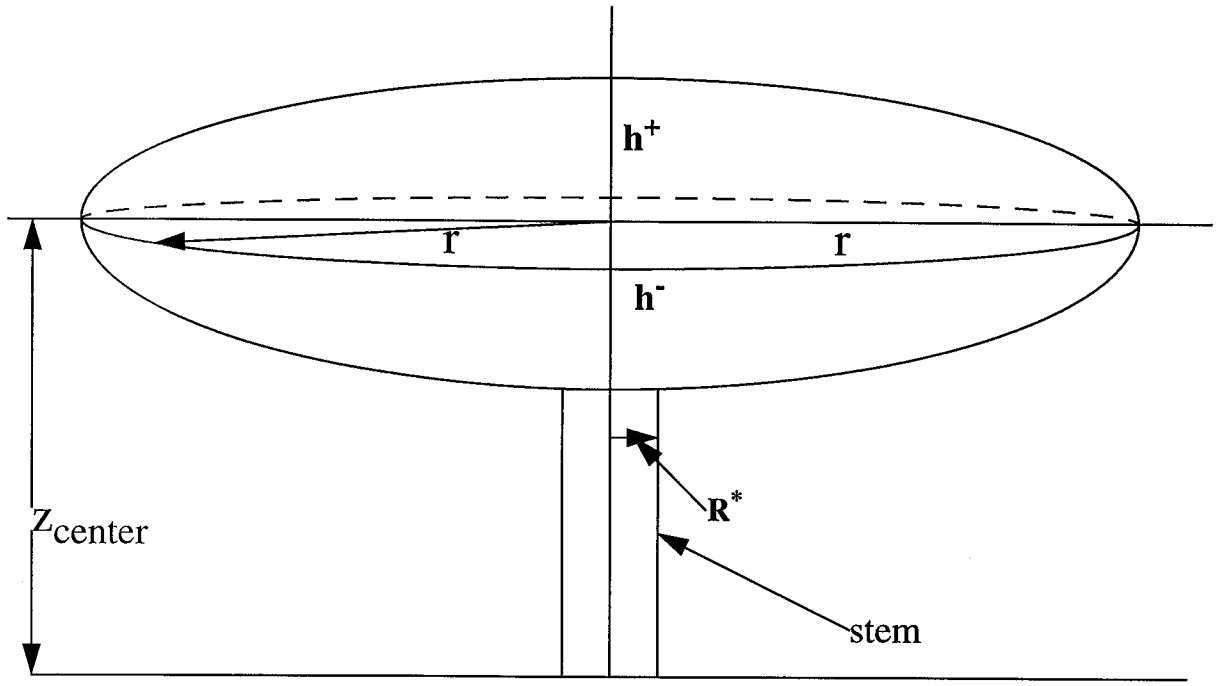

Figure 1. Idealized explosive cloud geometry.

The stem can be assumed to be a cylinder of height ($z-h^-$), and radius, R^*. In fact, many of the experiments conducted by Baskett and Freis (1997) on high explosives showed that the puff is approximately the union of simple three-dimensional objects. Conveniently, such an assumption produces simple algebraic expressions that simplifies the integration over space. The stem volume for a cylinder is:

$$V_s = \pi(z-h^-)\, R^{*2} \tag{14}$$

The puff density generated by high temperatures is approximately $\rho_p = \rho_a(T_a/\, T_p)$. For high explosives, $\rho_p = 0.06\ \rho_a$. According to Zheng et al. (1995), the Boussinesq approximation is valid if

$$(\bar{\rho}_a-\bar{\rho}_p)/\bar{\rho}_a < 0.1, \tag{15.a}$$

or

$$\bar{\rho}_p > 0.9\bar{\rho}_a. \tag{15.b}$$

Thus, the Boussinesq approximation is valid if $(T_p-T_a) < 0.11\ T_a$. Even for relatively cool hydrocarbon explosions, the Boussinesq approximation is not valid except as the puff asymptotically approaches its equilibrium height, H.

Because of the high initial temperatures generated by explosives, radiation is an important mechanism of heat loss. The present model assumes that the ambient atmosphere is an infinite

extent heat sink and the typical atmospheric emissivities, ε, are $0.65 < \varepsilon < 0.85$.

Rather than using the Reynold's stress averaged formulation valid only for constant density turbulence, the present model uses the Favre-averaged turbulent stress formulation, Libby and Williams(1980). The model for the puff and ambient turbulence will be discussed later as these terms are very important in determining the rate of rise of the puff.

The cartesian coordinate system is not the most convenient frame in which to describe the motion of a buoyant puff. Cylindrical coordinates are better because of the upward motion and the lateral or radial growth of the puff. For simplicity, this model assumes that azimuthal symmetry exists about the z axis.

The ordinary differential equations (ODEs) representing spatially averaged puff conservation of mass, momentum, and total energy are obtained by integrating the governing partial differential equations over space. There are two relevant boundaries: 1. the discontinuity of the hot puff and the ambient atmosphere interface, and 2. the boundary at infinity. At the puff centerline, the flow in the radial direction is zero because of symmetry; likewise, for the gradients in temperature, pressure, and density. Because of entrainment and turbulent mixing, any local gradients within the puff can be assumed to rapidly dissipate, and uniform values of the puff dependent variables rapidly establish. Across the moving puff-atmosphere interface, there are jump conditions that must be satisfied. At a sufficiently large distance from the puff, the explosion exerts no influence upon the atmosphere.

Because the puff-atmosphere boundary changes in time, the following Liebnitz rule is used:

$$(\partial/\partial t)\, {}_a\int^b f(x,t)dV = {}_a\int^b \partial f(x,t)/\partial t\, dV + f(x=b(t),t)\partial V(b)/\partial t - f(x=a(t),t)\partial V(a)/\partial t \qquad (16)$$

The volume element of integration is dV = dxdydz, V(b) and V(a) are the volumes at b and a, respectively.

Gauss's theorem for the integration of divergence of a vector, **A**, is given as:

$$\int (\nabla \bullet \mathbf{A})\, dV = \int \mathbf{A} \bullet \mathbf{n} dS \qquad (17)$$

where **n** is the outward unit normal vector and dS is an element of the surface area.

The volume integration is split into two parts. The first part is the ellipsoid representing the top and bottom halves of the cloud cap, and the second part is the stem. To accomplish the integrations of these surfaces, the outward normal vector at these surfaces is found, and the surface elements are constructed, then the averaged integration is completed.

The surface of an ellipsoid is given as

$$\Psi_s = (x^2 + y^2)/r_e^2 + z^2/h_e^2 - 1 = 0. \qquad (18)$$

and the surface of the stem is given as

$$\Psi_c = (x^2 + y^2) - z^2 = 0 \tag{19}$$

The normal vector for each case is given by

$$\mathbf{n}_m = \nabla\Psi_m / |\nabla\Psi_m|, \; m = 1,2. \tag{20}$$

To find the element of surface area for the ellipsoid and the stem, a unit vector is constructed from an origin to the surface in each of the three coordinate directions. Because this vector is constrained to be on the surface, it has only two independent degrees of freedom. The element of area is given by

$$dS = [(\partial\mathbf{k}/\partial q_1)\bullet(\partial\mathbf{k}/\partial q_1)(\partial\mathbf{k}/\partial q_2)\bullet(\partial\mathbf{k}/\partial q_2) - \{(\partial\mathbf{k}/\partial q_1)\bullet(\partial\mathbf{k}/\partial q_2)\}^2\,]^{1/2}\, dq_1 dq_2 \tag{21}$$

where (q_1,q_2) is an arbitrary point on the surface of S and dq_1 and dq_2 are the infinitesimal at (q_1,q_2). In all cases q_1 $(0 < q_1 < 2\pi)$ is the azimuthal angle about the z-axis and q_2 is the height of the ellipsoid, $(-h_e < q_2 < h_e)$. The other variable, r, in the radial direction is readily found because of the surface constraints.

2.4. Simplifying assumptions in the integrations

The variables, ρ_p, w_p, u_p, P_p, and e_p are assumed to be spatially uniform within both the cap and stem parts of the puff. Also, it is assumed that the variables, ρ_a,T_a, u_a, P_a, and e_a are independent of their x and y locations, but only depend on the height, z. A simplification can be made by assuming at the height, z, that $P_p(z) = P_a(z)$.

The surface areas projected on the radial and vertical directions can be given immediately as:

$$\mathbf{n}_e S_e = \pi\{2r_e h_e \mathbf{e_r} + 2\mathbf{e_k} r_e^2) \tag{22}$$

where $\mathbf{e_r}$ and $\mathbf{e_k}$ are the unit vectors in the r and z directions, respectively.

Next, the integrations over space can now be performed that, reduces the 3D PDEs to ODEs in time. Note, that the advective portion of the flux in strong conservative form makes these integrations quite simple. The advective flux vector,

$$\mathbf{F} = F_r\,\mathbf{e_r} + F_z\,\mathbf{e_k} \tag{23}$$

has components in the radial and vertical directions. The advective fluxes, in the radial and vertical directions, are given by:

$$F_r = [(\rho u), (\rho uu), (\rho uw), (\rho ue)]^T \tag{24.a}$$

and

$$F_z = [(\rho w), (\rho wu), (\rho ww), (\rho we)]^T \quad (24.b)$$

for the conservation of mass, radial momentum, vertical momentum, and total energy, respectively.

Because the puff boundary is growing laterally and vertically at some unspecified velocity, **s**,

$$\mathbf{s} = \{s_r \mathbf{e_r} + s_z \mathbf{e_k}), \quad (25)$$

the advective velocity that comprises the flux on either side of the puff interface is shifted in order to coincide with the expanding and distorting interface.

The entrainment of a quantity, Q, is given in terms of fluxes of the mean variables. (Note, Q=1 when the mass conservation equation is considered.)

The mean value flux quantities are defined as:

$$\bar{f}_a = \bar{\rho}_a(\bar{u}_a - s_r)A_r + \bar{\rho}_a(\bar{w}_a - s_z)A_z, \quad (26)$$

$$\bar{f}_p = \bar{\rho}_p(\bar{u}_p - s_r)A_r + \bar{\rho}_p(\bar{w}_p - s_z)A_z ; \quad (27)$$

and the turbulent flux quantities as:

$$\bar{f}''_a = \overline{\rho''_a u''_a}A_r + \overline{\rho''_a w''_a}A_z , \quad (28)$$

$$\bar{f}''_p = \overline{\rho''_p u''_p}A_r + \overline{\rho''_p w''_p}A_z ; \quad (29)$$

The rate of entrainment mixing of Q is limited by the available projected area and difference in fluxes, $(f^a Q^a - f^p Q^p)$. This flux difference tends toward zero as the puff state variables tend toward the ambient atmospheric variables.

Summarizing, the ordinary differential equations representing the uniform averaged puff-atmosphere conservation of mass, momentum, and energy are given by:

$$d\bar{m}/dt = (\bar{f}_a - \bar{f}_p) + \eta\bar{\rho}_a dV/dt, \quad (30)$$

$$d(\overline{mu})/dt = (f_a\bar{u}_a - f_p\bar{u}_p) + (\overline{f''_a u''_a} - \overline{f''_p u''_p}) + \eta\bar{u}_p\bar{\rho}_a dV/dt, \quad (31)$$

$$d(\overline{mw})/dt = (\bar{\rho}_a - \bar{\rho}_p)gV + (f_a\bar{w}_a - f_p\bar{w}_p) + (\overline{f''_a w''_a} - \overline{f''_p w''_p}) + \eta\bar{w}_p\bar{\rho}_a dV/dt, \quad (32)$$

$$d(\overline{me})/dt = (f_a\bar{e}_a - f_p\bar{e}_p) + \varepsilon\sigma(T_p^4 - T_a^4)A_T + (\bar{\rho}_a - \bar{\rho}_p)gV\bar{w}_p + (\overline{f''_a e''_a} - \overline{f''_p e''_p}) + \eta\bar{e}\bar{\rho}_a dV/dt \quad (33)$$

where

$$m = \int \rho_p \, dV = \bar{\rho}_p V. \quad (34)$$

The term, $\eta\bar{\rho}_a dV/dt$, represents the so-called virtual mass addition term. Daly and Harleman (1966) show that as a body accelerates through a fluid, a force must be applied to that body as well as to the fluid pushed out of the way. This virtual mass term is different from a drag force that is typically dependent upon the square of the relative velocities of an object moving in a fluid. The virtual mass term is an added force representing the interaction of the body and the fluid, and constitutes an additional resistance to the body. Such a body in a fluid behaves as if it had a mass larger than its true mass. The constant, η, is about 0.40 to 0.50.

The combined radial surface area from both the hemisphere and stem are given as:

$$A_r = \pi r(|h^+| + |h^+|) + 2.\pi\, r^2 z^2/(r^2+z^2)\,), \tag{35}$$

$$A_z = 2\pi r^2 + \pi rz(2r/(r+z) - rz/(r^2+z^2)). \tag{36}$$

The surface area of the stem is small compared to that of the cap, and will be ignored. The total volume occupied by the puff is given as the sum of volume occupied by the cap and stem,

$$V = (2\pi/3)r^2(\,|h^+| + |h^-|\,) + \pi(z-h^-)\, r_{initial}^2 \tag{37}$$

The contribution of the stem volume is small in comparison to that of the cap, and will be neglected.

3.0. Puff cloud Growth Model

Previous researchers assumed that the explosive puff is a sphere that grows with a radius directly proportional to the height. The present mode's approach for the rate at which the interface expands is similar to that of Boughton and DeLaurentis (1987) and Zheng et al. (1995), with the main exceptions that the Boussinesq approximation is not used, and the cloud cap is allowed to distort from a sphere to an ellipsoid.

Recall that the conservation of mass is given by:

$$d\bar{m}/dt = A_r\,[\bar{\rho}_a(\bar{u}_a-\bar{s}_r) - \bar{\rho}_p(\bar{u}_p-\bar{s}_r)] + A_z\,[\bar{\rho}_a(\bar{w}_a-\bar{s}_r) - \bar{\rho}_p(\bar{w}_p-\bar{s}_r)] + \eta\bar{\rho}_a dV/dt. \tag{30}$$

The top and bottom halves of the cloud-cap are generated by upper and lower ellipsoids, whose surface is denoted as $\Im$.

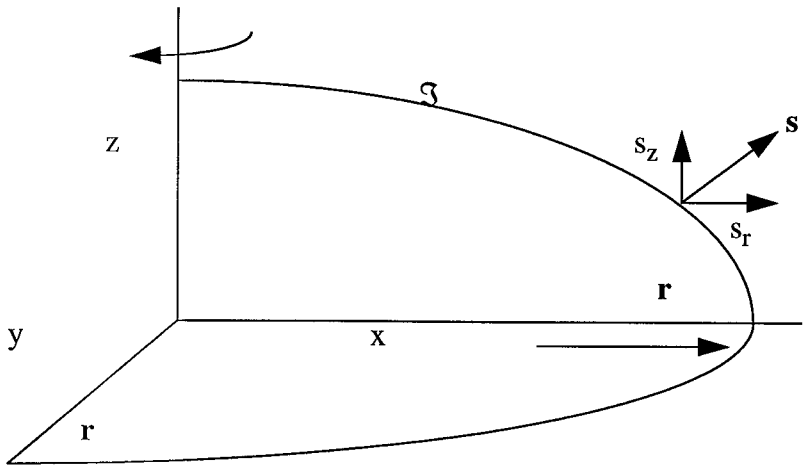

Figure 2. Schematic of the horizontal and vertical interface velocities.

The surface of the ellipsoid is denoted by $\Im$. The radius, r, of the ellipsoidal is constrained to have a constant value along the x and y axes. The height, $h^{\pm}$, of the ellipsoid along the x axis is constrained by the surface, $\Im$. So z is bounded by the surface

$$z = h^{\pm} [(1 - (x^2 + y^2)/r^2)]^{1/2} \tag{38}$$

The time rate of change is then given by

$$dh^{\pm}/dt = -(h^{\pm}/r)dr/dt. \tag{39}$$

The volume of the cap is given by

$$V = (2\pi/3)r^2 (h^+ + h^-), \tag{40}$$

and the volume rate of change is:

$$dV/dt = (2\pi/3)(2r(h^+ + h^-)dr/dt - r^2(dh^+/dt + dh^-/dt) = (2\pi/3)r(|h^+| + |h^-|)dr/dt. \tag{41}$$

Note that in the moving frame of the interface,

$$d\bar{\rho}_p /dt = -\nabla\bullet[\bar{\rho}(\mathbf{u} - \mathbf{s})]. \tag{42}$$

Subtracting Eq(42) from Eq(30) yields

$$s_r = 3\{ 2(\bar{\rho}_a\bar{u}_a - \bar{\rho}_p\bar{u}_p) \}/\{[(6-8\eta)\bar{\rho}_a + 2\bar{\rho}_p]\}. \quad (43)$$

and

$$dh^{\pm}/dt = s_z = -(h^{\pm}/r)dr/dt. \quad (44)$$

The latter two relations show that the top portion of the ellipsoid will elongate ($h^+ > z$) relative to the center of mass, and the lower portion ($h^- < z$) will flatten as the center z buoyantly rises. This is consistent with photographic observations of explosive clouds resulting from large explosions.This expression also includes the effect of the virtual mass term.

Boughton and DeLaurentis (1987) and Zheng et al. (1995) define the entrainment term to be:

$$E = \varphi\rho_a A_{sphere} * [(u_a - u_p)^2 + w_p^2]^{1/2} \quad (45)$$

where φ is a constant, $0.18 \leq \varphi \leq 0.28$, and

$$A_{sphere} = 4\pi r^2. \quad (46)$$

E, the entrainment, is the mass flux at the puff surface, assuming a spherical puff and the Boussinesq approximation, and disregarding the virtual mass contribution, i.e. $\eta = 0$.

With such assumptions, the time rate of change of the spherical radius is given by

$$s_r = \varphi[(u_a - u_p)^2 + w_p^2]^{1/2} \quad (47)$$

With the above assumptions, Eq (47), the speed at which the interface propagates is proportional to the entrainment.

3.1. Explosive cloud interaction with the atmosphere

The geometric center of the cloud cap will rise through different atmospheric layers, each possessing different "stabilities" as defined by vertical, wind speeds and directions. As with previous models, the present model relies upon atmospheric data such as temperature, wind velocity, and wind speed direction profiles as input. Estimates of the height of the surface, mixed, and boundary layers are assumed to be available.

This model assumes that at a height, z, representing the geometric center of the cloud cap, the cap experiences the wind speed, $u_a = u_a(z)$, and temperature, $T_a = T_a(z)$. The pressure, p_a, is found by integrating

$$dp_a/dz = -\bar{\rho}_a g \quad (48)$$

and $p_a = \Re\rho T$. (49)

3.2. Turbulence Models

The turbulent eddy viscosity and thermal conductivity are assumed to have two contributions: one arising from the ambient atmosphere, and the other from the puff itself. Observations of puffs show that there is a spectrum of eddy sizes that are predominantly short initially, and gradually become larger as the puff entrains successively more ambient atmosphere and cools. The ambient turbulent atmosphere can be treated by standard methods derived from measured quantities and a variety of stability conditions. The atmospheric turbulence contribution, $\overline{f''_a w''_a}$, $\overline{f''_a u''_a}$, and $\overline{f''_a e''_a}$ appearing in Eqs(31-33) of the present model uses the atmospheric turbulence models at various layers presented by Pielke (1984).

Stull (1988) pointed out that the local static stability is determined by the local lapse rate is misleading and often fails in the convective mixed layer. The rise of thermals from the surface or their descent from cloud tops depends on their excess buoyancy, not the ambient lapse rate. Stability must be determined with respect to water vapor content and the saturated adiabats. The virtual potential temperature is defined as

$$\theta_v = T_v + 0.00981*z \quad (50)$$

where

$$T_v = T(1 + 0.61q). \quad (51)$$

and q is the specific humidity (the mass of water vapor per unit mass of air). A simplifying assumption in the present model is that the specific humidity is zero, but this assumption can be readily relaxed if necessary.

Following Fleagle and Businger (1980), the non-dimensional Richardson number, Ri, which denotes the ratio of the buoyant energy to the shear kinetic energy, and is defined as:

$$Ri = g\partial \ln\theta_v/\partial z/ \left[(\partial u/\partial z)^2 + (\partial v/\partial z)^2 \right] \quad (52)$$

Fleagle and Businger (1980) classify the atmosphere as unstable (convective) for Ri<0, neutral for Ri = 0, and stable for Ri>0.

Stull (1988) points out that an unstable atmosphere is characterized by random updrafts and downdrafts. Within a random updraft, the puff can be accelerated upwards. Within a downdraft, the buoyant rise of the puff decelerates, behaving as if it were moving in a very viscous medium. However, in most circumstances, an unstable atmosphere instability is dominated by solar heating, and typically confined in a region from the surface to a mixed layer height.

Unstable atmospheric conditions are the most difficult to predict with the buoyant puff model. While commonly assumed that the time-averaged vertical atmospheric velocity, $\overline{w}_a = 0$, an

explosive puff within the unstable layers could experience transient updrafts or downdrafts. Unless some turbulence data regarding these velocities are provided, the behavior of the puff under unstable conditions is very uncertain. This issue will be discussed in more detail with the puff-atmosphere turbulence model section.

3.2.1. Puff-Atmosphere Turbulence Model

In contrast to the well-studied atmospheric turbulence, the puff-atmospheric turbulence model is a rather uncharted area. Libby and Williams (1980) and Ermak (1990) have pointed out that clouds of either hot or cold gases can enhance or suppress turbulent mixing. The puff-atmospheric turbulence model involves those fluctuating terms having the following structure

$$A_i[\,\overline{\rho''}_p\overline{Q''}_p\overline{w''}_p\,] \tag{53}$$

All turbulence models require a means of closure. The puff-atmospheric interface is quite turbulent, so any particle at or near this edge may be inside or outside of the puff at any instant of time. To avoid calculating very detailed complex higher order closure models, the following assumptions were made:

$$\overline{\rho''}_p = \overline{\rho}_p - \overline{\rho}_a\,, \tag{54}$$

$$\overline{Q''}_p = \overline{Q}_p - \overline{Q}_a, \tag{55}$$

$$\overline{w''}_p = \overline{w}_p \quad (\text{assuming } \overline{w}_a = 0) \tag{56}$$

$$\overline{u''}_p = \overline{u}_p - \overline{u}_a \tag{57}$$

$$\overline{e''}_p = \overline{e}_p - \overline{e}_a$$

The contribution to the puff-atmosphere projected on the i-th axis is given by:

$$A_i[\,\overline{\rho''}_p\overline{u''}_{i,p}\overline{u''}_{jp}] = k_{p\text{-}a}A_i\,(\overline{\rho}_a - \overline{\rho}_p)(\overline{u}_{i,p}-\overline{u}_{i,a})(\overline{u}_{j,p}-\overline{u}_{j,a}) \tag{58}$$

$$A_i[\overline{\rho''}_p\overline{e''}_p\overline{u''}_{i,p}] = k^e_{p\text{-}a}A_i\,(\overline{\rho}_p - \overline{\rho}_a)(e_p-\overline{e}_a)(\overline{u}_{i,p}-\overline{u}_{i,a}) \tag{59}$$

where A_i is either the r or z projected area, $k_{p\text{-}a}$ and $k^e_{p\text{-}a}$ are the effective eddy viscosity and turbulent thermal conductivities, respectively. These constants, $k_{p\text{-}a}$ and $k^e_{p\text{-}a,}$ were determined empirically by comparing the model results with the observed puff height of the Roller Coaster experiments, Church (1969). For simplicity, it was assumed that $k^e_{p\text{-}a,} = k_{p\text{-}a}$.

$k_{p\text{-}a}(z)$

Note that these turbulence terms in the two momentum equations involve products of the velocity differences, and can be interpreted as "turbulent drag" terms. These "drag" terms

render the system of ODEs nonlinear. However, unlike the atmospheric turbulence, the puff-atmospheric turbulence terms, Eqs(58-59) vanish when the puff dependent variables approach atmospheric values; this property is consistent with the assumption made earlier. Entrainment, the atmospheric turbulence, and puff-atmospheric turbulence are considered to be the dissipation terms whose magnitudes determine the time at which the puff reaches a steady state height.

Atmospheric stability plays a very important role in governing the rate of rise of the puff and in determining the time required for a puff to reach a steady state height. The puff-atmospheric dissipation terms, $k_{p\text{-}a}$ and $k^{e}_{p\text{-}a}$, are assumed to be a function of the local Richardson number, Ri, and height, z, above the surface, similar to the atmospheric turbulence models.

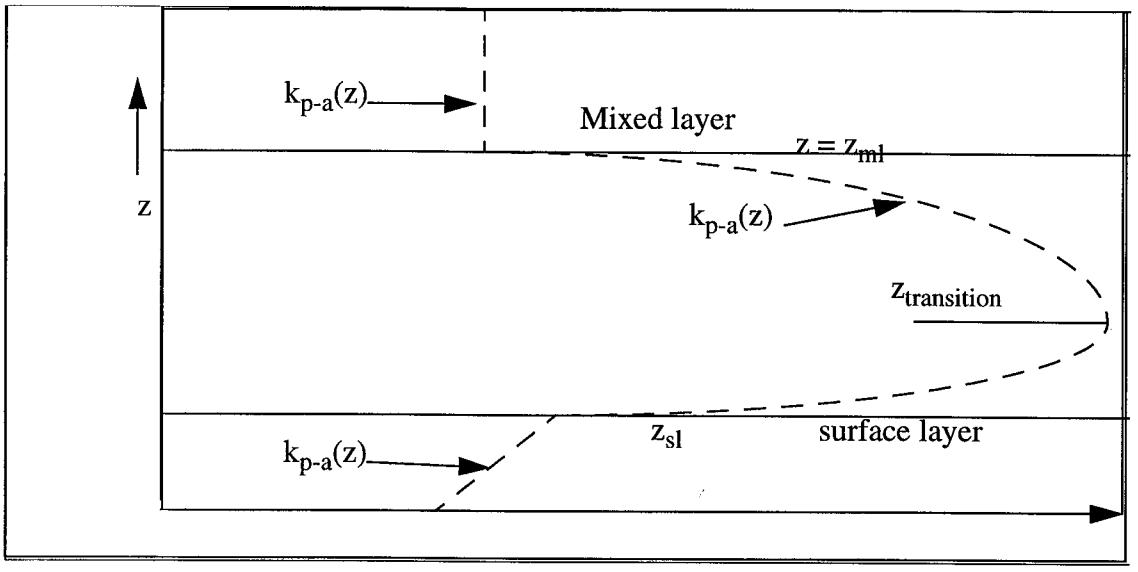

Figure 3. Schematic of the dependence of $k_{p\text{-}a}(z)$ versus z from the surface to the mixing layer.

The height of the surface and mixed layers is a function of time of day, degree of surface heating, surface type, albedo, soil moisture and latitude. In summer months, the mixed layer characterized by strong convective heating can be anywhere from 1,000 to 2,000 m above the surface. On clear nights, near dawn, the convective mixing of the atmosphere ceases, and the atmosphere is very stable with the mixing depth from 100 to 300 m above the surface. The above model is convenient to characterize the various atmospheric stability conditions. The present puff rise model assumes that the atmospheric soundings are available to determine the initial conditions.

An eddy diffusivity coefficient, $k_{p\text{-}a}(z)$, is assumed to be a function of height, z. From the surface to the top of the surface layer, $k_{p\text{-}a}$ is assumed to vary linearly with z. From the surface layer to the transition height

$$z_{transition} = z_{sl} + (z_{ml} - z_{sl})/3 \quad (60)$$

$k_{p\text{-}a}$ becomes a maximum at $z_{transition}$, and then reduces to a smaller value at $z = z_{ml}$. Above h_{ml}, $k_{p\text{-}a}$ is assumed to be constant.

In general, a puff that has lost most of its buoyant momentum is trapped at the mixed layer. The critical feature determining whether a puff will be trapped at this layer, or punch through it, depends upon the excess vertical momentum of a puff. For a stable atmosphere, an explosion with a certain mass will equilibrate at the mixed layer, but an explosion with double the mass may punch through and equilibrate at a much larger height. Because of the initial temperature difference, an exploding gasoline vapor cloud may equilibrate at a much lower height than a TNT explosion.

If $T_{puff}(h_{ml}) > T_{atmosphere}(h_{ml})$, the puff will have excess vertical momentum and may punch though the mixed layer and find a different stabilizing height; otherwise, the puff will equilibrate at the mixed layer height.

By experimentation, the puff-atmospheric eddy coefficients were found to increase with increasing Richardson number whereas the ambient atmospheric turbulence decreases with increasing Richardson number. In the unstable atmospheric conditions, the ambient atmospheric eddy coefficients increased with decreasing Richardson number, and the puff-atmospheric eddy coefficients decreased with decreasing Richardson number. A research effort to understand this phenomenon is beyond the scope of the project goals. At present, there has not been any detailed studies or models formulated to understand the turbulence of hot gases mixing with the cooler atmosphere.

3.2.2. The puff-atmospheric mixing coefficients

Experimentation with the model showed that the puff-air turbulence and the effective cross-sectional area are the dominate factor determining both the rate at which the puff looses its excess buoyancy. By fine tuning the adjustable multiplicative factors for both terms, it is possible to match the puff history rise.

The determination of the puff-atmospheric turbulence parameters is basically an inverse problem. Church (1969) and Baskett and Freis(1997) have reported the measured puff cloud top heights as a function of time for varying amounts of explosive and atmospheric stability conditions. Ideally, the inverse problem could be solved by time marching the set of nonlinear ODEs of the present model simultaneously and adjusting the parameters simultaneously to minimize the least squares errors between the predicted puff cloud heights and the observed heights. However, such an approach requires huge demands upon the computer resources, and a simpler approach was used. Rather each experiment was optimized separately to obtain a reasonable average of the parameters. The experiments used from 6.4 to 1019 kg TNT equivalent amounts of explosive mass. In a sense, the parameters were interpolated for this range of explosive. Whether such parameters are reasonably valid beyond range for which they were adjusted can only be determined by future experiments. In addition, there is a concern that

three dimensional effects can become quite important for very large explosions. Such effects were ignored in order to obtain such a simple model.

Table 1 lists the maximum and minimum values for the puff-atmospheric eddy viscosity and area multipliers. Model experimentation revealed that for very stable atmospheres, the puff-atmospheric viscosity and area multiplicative factors needed to be increased with increasing positive Ri number, and visa versa.

Intuitively, this is physically consistent. An unstable atmosphere is very turbulent, and in such an atmosphere, the puff is being buffeted by strong eddies that induce mixing rapidly, so the puff-generated turbulence is of minor importance. However the presence of finite duration updrafts or downdrafts can either accelerate or decelerate the puff dramatically,

For neutral or stable conditions, the atmospheric turbulence plays a decreasing role in mixing with increasing positive Ri number. In very stable atmospheres with Ri > 0.5, the puffs are observed to equilibrate rapidly to the mixed layer that can be relatively close to the surface. Thus, the hot puff must dissipate its heat rapidly, assuming radiation loss is important only in the initial time when its temperature > 2,000 K. This implies that entrainment and the puff generated turbulence are the dominant mechanisms. So for increasing Ri, the effective area and puff eddy dissipation would increase with Ri number.

In Table 1, $k_{p\text{-}a} = k^e_{p\text{-}a}$ are listed as a maximum and minimum values for the various ambient atmospheric Richardson numbers. Likewise, the effective area coefficient, Ξ, is assumed to vary with height similar to the puff-atmospheric eddy viscosity coefficients. These parameters were fine-tuned to the 63.6 kg TNT equivalent of the Roller Coaster experiments. In a separate section, these parameters will be adjusted for larger or smaller explosions.

Table 1: Puff-atmospheric parameters calibrated for 63.6 kg TNT explosions

Attribute	-0.5<Ri<-0.1	-0.1≤Ri<0	0.0≤Ri<0.5	0.5≤Ri<0.8	0.8≤Ri≤1.0	Ri > 1.0
$k_{p\text{-}a}$(max)	0.08	0.090	0.16	1.09	2.05	5.0
$k_{p\text{-}a}$(min)	0.06	0.075	0.10	1.05	1.70	1.75
Ξ(max)	0.50	0.53	1.03	1.10	1.20	2.25
Ξ(min)	0.40	0.42	0.98	1.02	1.03	1.5

This table illustrates that mean flow entrainment and "turbulent drag" upon the hot puff increases with increasing Richardson number. This is physically consistent with the experimental observations that a puff looses its excess buoyancy rapidly in a stable atmosphere, but rises higher in a less stable atmosphere. In seperate model calculations, it was observed that for a very stably layered atmosphere, that doubling the explosive mass causes the puff to equilibrate at a significantly higher layer, while halving the explosive mass causes the puff to

equilibrate at a lower height. Similarly, if the lower layers of the atmosphere are unstable, say for the first kilometer above the surface, the standard atmospheric model of the upper portions of the atmosphere tend to have more stable atmospheric conditions. So a puff generated by a rather large explosive mass rising in the upper layers will entrain cooler atmospheric air and encounter a "turbulent drag" that eventually slows and stops a puff from rising further.

3.3. Semi-analytic solutions of the buoyant puff model

To simplify the numerical implementation of the buoyant puff model, the puff pressure is assumed at the height, z, to be equal to the pressure of the ambient atmosphere at the same height. The conservation of mass equation, when integrated, gives the mass of the puff at any time.

The conservation equations for total vertical and radial momentum and total energy can be simplified by subtracting the conservation of mass equation multiplied by the appropriate quantity.

Consider any puff variable, Q.

Define fluxes

$$F_a = \bar{\rho}_a [A_r (\bar{u}_a - \bar{s}_r) + A_z (\bar{w}_a - \bar{s}_z)], \tag{61}$$

$$F_p = \bar{\rho}_p [A_r (\bar{u}_p - \bar{s}_r) + A_z (\bar{w}_p - \bar{s}_z)]. \tag{62}$$

$$\text{So } dm_p/dt = \eta \bar{\rho}_a dV/dt - (F_p - F_a) \tag{63}$$

Using the relation,

$$m_p dQ_p/dt = d(m_p Q_p)/dt - Q_p dm_p/dt, \tag{64}$$

the following ODEs for the puff vertical, horizontal, and energy equations are obtained:

$$m_p dw_p/dt + \{F_p + k_{p-a}(\bar{\rho}_a - \bar{\rho}_p)\{A_r(u_p - u_a) + A_z(w_p - w_a)\}(]w_p - w_a) = (\bar{\rho}_a - \bar{\rho}_p)gV - K_w^{atm} \tag{65}$$

$$m_p du_p/dt + \{F_p + k_{p-a}(\bar{\rho}_a - \bar{\rho}_p)\{A_r(u_p - u_a) + A_z(w_p - w_a)\}](u_p - u_a) = K_u^{atm} \tag{66}$$

$$m_p de_p/dt + \{F_p + k^e_{p-a}(\bar{\rho}_a - \bar{\rho}_p)\{A_r(u_p - u_a) + A_z(w_p - w_a)\}](e_p - e_a) = (\bar{\rho}_a - \bar{\rho}_p)gVw_p + K_e^{atm} - \varepsilon\sigma (T_p^4 - T_a^4)A_T \tag{67}$$

In a sufficiently small time interval, Δt, the puff mass, m_p, the volume, V, the density difference

term, $\Delta\bar{\rho}$, the projected surface areas, A_z and A_r, the interface velocities, s_r and s_z, and the turbulence parameters, $k_{p\text{-}a}$ and $k^e_{p\text{-}a}$, can be considered slowly varying after the radiative term becomes negligible ($T_p < 2000$ K). If this be the case with a sufficiently small time interval, Δt, analytic expressions can be obtained.

For convenience, the atmospheric turbulence is defined as

$$\Lambda_{atm} = -K_{atm}(Ri)(\partial\bar{u}_a/\partial z). \tag{68}$$

$$\text{and } F' = F_a + \Delta\bar{\rho}\, k_{p\text{-}a}A_r\Delta u. \tag{69}$$

A rearrangement of the vertical velocity ODE gives

$$dw_p/ (\Delta\bar{\rho}\, k_{p\text{-}a}A_z\, \bar{w}_p^{\,2} + F'\bar{w}_p + (\Lambda_{atm} - \Delta\bar{\rho}\, gV) + dt/M_p = 0 \tag{70}$$

Under the above assumption, this ODE can be integrated to yield the following expression:

$$\bar{w}_p = [\delta - F' + (\delta + F')*\exp(-\delta\Delta t/M_p)\,]/\{\,[1-\kappa_o\exp(-\delta\Delta t/M_p)]\Delta\bar{\rho}\, k_{p\text{-}a}A_z\,\} \tag{71}$$

$$\text{where } \delta = [\,(F')^2 - 4(\Delta\bar{\rho}gV-\Lambda_{atm})(\Delta\bar{\rho}\, k_{p\text{-}a}A_z)\,]^{1/2}. \tag{72}$$

$$\text{and } \kappa_o = -\log(\,\delta + F'). \tag{73}$$

Assume $0 < \Delta\bar{\rho} \le 0.5\bar{\rho}_a$. The expression for w_p simplifies, after expanding δ to yield:

$$\bar{w}_p \cong [\,2(\Delta\bar{\rho}\, gV - \Lambda_{atm})/F' + F'\exp(-3\bar{u}_a\Delta t/h)\,]/(\,[1-\kappa_o\exp(-3\bar{u}_a\Delta t/h)] \tag{74}$$

w_p is directly proportional to the difference of the buoyant force and atmospheric dissipation, and inversely proportional to the surface area and wind velocity. The greater the ambient wind speed, $\bar{u}_a$, the faster does the vertical velocity decay. A similar analytic expression exists for the time dependency of $\bar{u}_p$, except the buoyant force term is absent.

Assuming that the radiation transport is small, the energy equation can be linearized. For convenience, define:

$$F'' = \{F_p + k^e_{p\text{-}a}(\bar{\rho}_a - \bar{\rho}_p)\{A_r(u_p-u_a)+A_z(w_p-w_a)\}] \tag{75}$$

and

$$G = (\bar{\rho}_a - \bar{\rho}_p)gVw_p - K_e^{atm} - \varepsilon\sigma\,(T_p^{\,4} - T_a^{\,4})A_T. \tag{76}$$

The solution to the differential equation

$$de_p/dt + (F''(e_p-e_a) + G) = 0 \tag{77}$$

is

$$e_p = e_a + (\kappa_e \exp(-\delta' \Delta\tau / M_p) - G)/F'' \quad (78)$$

This expression is not valid for early times when radiative dissipation is very important. As with the expression for w_p, increasing wind speed decreases the time for the temperature of the puff to approach the ambient temperature, as well as the role of atmospheric heat dissipation. Also, the larger the mass of the puff, the longer is the time required the puff energy to dissipate.

While these analytic expressions are useful for gaining physical insight, it must be emphasized that these nonlinear, coupled ODEs were essentially decoupled and the dimensions of the puff were assumed to be constant. This is only true if sufficiently small time steps are used.

Again, the present model assumes that

$$\bar{p}_p = \Re \bar{\rho}_p \bar{T}_p = \bar{p}_p = \Re \bar{\rho}_a \bar{T}_a . \quad (79)$$

A necessary and sufficient condition for stable, physically acceptable solutions is that the puff turbulence terms be positive definite. Otherwise, the solutions would become numerically unstable. From these simplified expressions, it is clear that for sufficiently long time, there exists a height H such that

$$w_p(H) \rightarrow 0 = w, \quad (80)$$

$$u_p(H) \rightarrow u_a(H), \quad (81)$$

$$\rho_p(H) \rightarrow \rho_a(H), \quad (82)$$

$$T_p(H) \rightarrow T_a(H). \quad (83)$$

3.4. Mass adjusted puff-atmospheric turbulence parameters

The atmospheric stability and related puff-atmospheric turbulence parameters are very important in determining the rise history of an explosive puff. The other important parameter, for a given class of explosives, is the TNT equivalent of a mass of explosive.

Church (1969) shows that the two minute cloud-top heights when plotted logarithmically against the TNT equivalent of explosive mass is fairly linear. Adjusting to the MKS units, the two minute cloud-top heights are bounded by the following curves:

$$z = 86.62 (m_{TNT})^{0.25} \quad (84.a)$$

$$= 125.66 (m_{TNT})^{0.25} \quad (84.b)$$

or

$$= 74.33 (m_{TNT})^{0.293} \quad (84.c)$$

where m_{TNT} ia the TNT equivalent of explosive in kg, and the height z is in meters.

A reasonable compromise choice for the two minute cloud top height is

$$z = 95(m_{TNT\ equ})^{0.25} \tag{85}$$

In order to place upper and lower bounds, it is convenient to obtain a semi-analytic expression for the two-minute cloud-top heights. Let the cloud center of mass be defined as:

$$z = \int w(t)dt \tag{86}$$

Using as the starting point, the expression for w(t), Eq(71), z is then

$$z = z_0 + 1/ (k_{p-a}\Delta\rho A_z) \{ (\delta\text{-}F')t - (2F'/\delta)\log(1 - k_0\exp(-\delta\, \Delta t/M) \} \tag{87}$$

Specifying z at 2 minutes (120 sec) and assuming a 10% error bar around the value of z_2, an upper and lower bound to k_{p-a} can be estimated. This model assumes that at 2 minutes, $\Delta\rho = 0.5\rho_a$, $M = 0.5\rho_a(\alpha z)^3$, and s_r and s_z are given by Eq(43) and (44), respectively.

Thus,

$$k_{p-a} = \{(\delta - F') t - (2F'/\delta) \log(1 - \kappa_0\exp(-\delta t/M)) \} / (z_2 - z_0)(A_z \Delta\rho) \tag{88}$$

where z_2 is allowed to vary by 10% about its mean value.

3.5. Required input data

This model requires information about the initial atmospheric conditions including:

- the height of the surface and mixing layers,
- the surface pressure,
- the u and v wind velocity and temperature profiles,
- estimates of the Obukhov length scale, and the friction velocity, u_*.

These parameters are used to construct turbulence models for the ambient atmosphere as well as that of the puff-atmospheric interaction.

Other relevant data are:

- the amount of explosive,
- its chemical composition class (high explosive, propellent, or hydrocarbon),
- the initial coordinates (x,y,z) of the explosion.

The default values for the maximum and minimum values of the atmospheric turbulence and effective area multiplier are one, but these parameters can be readily changed to suit a particular situation.

4.0. Model Comparison to Experiments

4.1. Roller Coaster Series

The model results were primarily compared and calibrated against the series of Roller Coaster high explosive experiments undertaken at Tonopah Test Range at the Nevada Test Site in May and June, 1963. These shots were performed from dusk to dawn under a variety of atmospheric stability conditions. The height of the cloud tops was obtained either by photographs or by theodolite tracking measurements. A vertical illuminated grid was erected to measure photographically the puff tops at various times, up to 5 minutes after the explosion. The ambient temperature and wind profiles were measured up to 600 m from the surface at a station 3.6 km from ground zero. These data and the observed heights at various times were documented by Church (1969).

The results presented here are not sequential; rather they are grouped by atmospheric stability conditions as indicated by the Richardson number in the following order: neutral ($0.0 \leq Ri \leq 0.10$), mildly stable ($0.10 < Ri \leq 0.35$), very stable ($Ri > 0.35$), and unstable ($-0.5 \leq Ri < 0.0$). Several of the Roller Coaster shots exhibited multiple stability layers, most of which occurred in the night when the ground had radiatively cooled leaving the upper layers with nearly neutral conditions. In all the figures to be presented, the meteorological data (wind speed, temperature, and shear angle versus height) will be given.

4.1.1. Neutral Shots ($0.00 \leq Ri < 0.10$)

Figure 4 shows the height of the puff top vs. time for Roller Coaster 3 (63.6 kg explosive) that was measured up to 5 minutes after the explosion. Roller Coaster 3 has a very narrow range of Ri numbers ($0.0 \leq Ri \leq 0.02$). The puff top height and radius at 5 minutes is 581 m and 57 m, respectively.

Figure 5 shows the height of the puff top vs. time for Roller Coaster 11 (63.6 kg explosive) that was measured up to 5 minutes after the explosion. Roller Coaster 11 has a very narrow range of Ri numbers ($0.01 \leq Ri \leq 0.02$).

The last measurement taken 3 minutes after the explosion is at a height of 378 m above the surface in excellent agreement with the predictions. Because of the neutral conditions, the puff top rises to a height of 552 m after 5 minutes after the explosion. The puff top height and radius at 5 minutes is 552 m and 46.5 m, respectively.

Figure 6 shows the height of the puff top vs. time for Roller Coaster 12 (63.6 kg explosive) that was measured up to 5 minutes after the explosion. Roller Coaster 12 has a very narrow range of Ri numbers ($0.06 \leq Ri \leq 0.07$). The puff top rises to a height of 643 m after 5 minutes after the explosion. The puff top height and radius at 5 minutes is 643 m and 61.5 m, respectively.

Interestingly, Roller Coaster 3 11, and 12 events used the same amount of explosives, 63.6 kg, under near neutral conditions. Yet the heights after 5 minutes were: 581, 552, and 643 m, respectively. While the behavior of Roller Coaster 3 and 11 are practically identical, Roller Coaster 12 is rather odd; perhaps during the time the meteorological parameters were measured

and the explosion was set off, the wind and temperature profiles may have changed somewhat. Subtle differences in the atmospheric stability may account for this 90 m variation in puff top height.

4.1.2. Mildly Stable Shots ($0.10 < Ri \leq 0.35$)

The following set of experiments were conducted in mildly stable atmospheres having different layers as denoted by the Ri number. For this set of experiments, two methods were attempted. One method height-averaged the variations of the Ri number, and the other method used the actual variations in each layer. It appears that, at least for these set of experiments, a closer match of the experimental rise times was obtained when the details of each Ri layer was used.

Figure 7 shows the height of the puff top vs. time for Roller Coaster 2 (63.6 kg explosive) that was measured up to 4 minutes after the explosion. Table 2 shows the dependency of Ri number

Table 2: Richardson Number versus Height for Roller Coaster 2

Height (m)	Ri
0 -95	0.02
95 - 164	0.07
164-250	0.09

with height at three different layers. The puff top height and radius at 5 minutes is 250 m and 21.2 m, respectively.

Figure 8 shows the height of the puff top vs. time for Roller Coaster 4 (727 kg explosive) that was measured up to 5 minutes after the explosion. Roller Coaster 4 exhibited three stability layers presented in Table 3.

Table 3: Richardson Number versus Height for Roller Coaster 4

Height (m)	Ri
0-55	0.35
55- 550	0.03-0.06
> 550	0.01

The puff top height and radius at 5 minutes is 560 m and 88.1 m, respectively.

Figure 9 shows the height of the puff top vs. time for Roller Coaster 9 (727 kg explosive) that was measured up to 5 minutes after the explosion. Roller Coaster 9 had only one atmospheric layer: from 0-200 m, Ri = 0.10. The puff top height and radius at 5 minutes is 195 m and 94.3

m, respectively.

Figure 10 shows the height of the puff top vs. time for the Doubletrack shot (53.6 kg) that was measured only up to 3 minutes after the explosion. Two atmospheric layers were documented in Table 3. The puff top height and radius at 5 minutes is 210 m and 14.1 m, respectively.

Table 4: Richardson Number versus Height for Doubletrack

Height (m)	Ri
0 - 73	0.29
73-215	0.10

4.1.3. Very Stable Shots (Ri > 0.35)

Figure 11 shows the height of the puff top vs. time for the Roller Coaster 5 (254 kg) that was measured up to 5 minutes after the explosion. Roller Coaster 5 exhibited four stability layers. The stability layers for this shot is presented in Table 5.

Table 5: Richardson Number versus Height for Roller Coaster 5

Height (m)	Ri
0 - 65	0.29
65- 170	0.34
170 - 345	0.11
> 345	0.08

The puff top height and radius at 5 minutes is 410 m and 30.5 m, respectively.

Figure 12 shows the height of the puff top vs. time for the Roller Coaster 6 (254 kg) that was measured up to 5 minutes after the explosion. Roller Coaster 6 exhibited four stability layers presented in Table 6. The puff top height and radius at 5 minutes is 531 m and 24 m, respectively.

Table 6: Richardson Number versus Height for Roller Coaster 5

Height (m)	Ri
0 -53	2.1
53-110	0.95

Table 6: Richardson Number versus Height for Roller Coaster 5

Height (m)	Ri
110 - 180	0.34
> 180	0.09

Figure 13 shows the height of the puff top vs. time for the Roller Coaster 7 (63.6 kg) that was measured up to 5 minutes after the explosion. Roller Coaster 7 exhibited three stability layers presented in Table 7.

Table 7: Richardson Number versus Height for Roller Coaster 7

Height (m)	Ri
0 - 162 m	1.10
162 - 300 m	0.34
300 - 360 m	0.12

The puff top height and radius at 5 minutes is 354 m and 15.3 m, respectively.

Figure 14 shows the height of the puff top vs. time for the Roller Coaster 8 (63.6 kg) that was measured up to 5 minutes after the explosion. Roller Coaster 8 exhibited five stability layers, see Table 8.

Table 8: Richardson Number versus Height for Roller Coaster 8

Height (m)	Ri
0 - 127	0.63
127-273	0.94
273 - 318	0.35
318 - 381	0.16
381- 500	0.10

The puff top height and radius at 5 minutes is 667 m and 32.2 m, respectively.

Figure 15 shows the height of the puff top vs. time for the Roller Coaster 10 (63.6 kg) that was measured up to 5 minutes after the explosion. Roller Coaster 10 exhibited several stability layers, see Table 9.

Table 9: Richardson Number versus Height for Roller Coaster 10

Height (m)	Ri
0-49	0.91
49- 143	0.59
143-283	0.25
283-320 m	0.32

The puff top height and radius at 5 minutes is 311 m and 19.4 m, respectively.

Figure 16 shows the height of the puff top vs. time for the Clean Slate 2 (1019 kg) that was measured up to 5 minutes after the explosion. Clean Slate 2 one stability layer, Ri = 0.87 from the surface to a height of 440 m. The puff top height and radius at 5 minutes is 427 m and 130 m, respectively.

Figure 17 shows the height of the puff top vs. time for the Clean Slate 3 (1019 kg) that was measured up to 5 minutes after the explosion. Clean Slate 3 one stability layer, Ri = 0.87 from the surface to a height of 510 m. The puff top height and radius at 5 minutes is 506 m and 57 m, respectively.

4.1.4. Unstable Cases ($-0.50 \leq Ri < 0.0$)

Analysis of explosions in unstable atmospheres is difficult because it is difficult to determine whether the transient explosion occurs in an updraft or downdraft. The vertical wind profiles were not measured during such events. However, two shots were undertaken that appears to have occurred in updraft conditions.

Figure 18 shows the height of the puff top vs. time for the Roller Coaster 1 (63.6 kg) that was measured up to 5 minutes after the explosion. Roller Coaster 1 exhibited five stability layers presented in Table 10.

Table 10: Richardson Number versus Height for Roller Coaster 1

Height (m)	Ri
0 - 25	-0.15
25 - 100	-0.02
100 - 155	-0.12
155 - 252	-0.08

Table 10: Richardson Number versus Height for Roller Coaster 1

Height (m)	Ri
252-730	-0.14

The puff top height and radius at 5 minutes is 727 m and 80.7 m, respectively.

Figure 19 shows the height of the puff top vs. time for the Clean Slate 1 (483 kg) that was measured up to 5 minutes after the explosion. Clean Slate 1 exhibited six stability layers, see Table 11.

Table 11: Richardson Number versus Height for Clean Slate 1

Height (m)	Ri
0 - 25	-0.15
25 - 130	-0.12
130 - 185	-0.07
185 - 215	-0.10
215 -780	-0.14
780 - 1020	-0.08

The puff top height and radius at 5 minutes is 1010 m and 82.1 m, respectively.

4.1.5. Statistical analysis of the model predictions against the Roller Coaster experiments

Table 12 lists the absolute residual error and the normalized root mean square error of the measured Roller Coaster field experiments against the prediction of the present model. Church (1969) listed the heights of the cloud tops at the following intervals: 0.5, 1.0, 2.0, 3.0, 4.0, and 5.0 minutes after detonation. The average absolute residual error (AARE) is defined as:

$$AARE = \Sigma_{i=1} \, | z_{model}(t_i) - z_{field}(t_i))|/(z_{field}(t_i) \, N_{obs}] \qquad (89)$$

Table 12: Average absolute residual error of cloud top heights of model predictions and field observations

Experiment Name	AARE
Roller Coaster 1	0.08736

Table 12: Average absolute residual error of cloud top heights of model predictions and field observations

Experiment Name	AARE
Roller Coaster 2	0.13414
Roller Coaster 3	0.13228
Roller Coaster 4	0.13246
Roller Coaster 5	0.09846
Roller Coaster 6	0.07110
Roller Coaster 7	0.04478
Roller Coaster 8	0.12326
Roller Coaster 9	0.0274
Roller Coaster 10	0.14133
Roller Coaster 11	0.05437
Roller Coaster 12	0.12491
Clean Slate 1	0.05587
Clean Slate 2	0.12903
Clean Slate 3	0.13184
Double Track	0.13470

The average absolute residual error over these set of experiments is 0.1014. Upon examining the plots, most of the errors resulted from the mismatch between the predicted values and the early time measurements, denoted by the X's. However, the asymptotic behavior is extremely good; within 5% in most instances.

4.2. Site 300 Experiments

Baskett and Freis (1997) reported the setup and analysis for a series of seven high explosive detonations conducted at LLNL's Site 300 facility to study the atmospheric dispersion of (Be) beryllium from explosions. Although the primary goal of these experiments was to measure the Be particulate dispersion, they also measured the cap cloud heights and cap cloud diameters as a function of time after detonation. They observed the position and size of the cap cloud depends upon the amount of explosive, the physical arrangement of the shot, and the meteorological conditions. Also, they observed that the cap cloud distorts from an initial spherical shape into one which upon rising distorts into an elongated shape.

4.2.1. Model Comparison with the Site 300 Experiments

The simulations of the Site 300 shots will be done sequentially, according to the date of the shots. As with the Roller Coaster experiments analyzed by Church (1969), the Site 300 shots are typically small explosions, ranging from 6.4 to 31 kg of high explosives, and conducted over a range of atmospheric stability conditions.

Shot 413-a

This shot was conducted 13 March, 1991 15:43 PST using 23 kg of high explosive. Table 13 shows the atmospheric stability layers as derived from the meteorological data. The average wind speed at 10m was 11.5 m/s.

Table 13: Height vs. Ri for shot 413-a

Height (m)	Ri
0-76	-0.112
76-230	-0.049
230-533	-0.034
533-843	0.122
850-1000	0.110

Figure 20 shows the history of the rise vs time for both the model and experimental observations.

Shot TG1-17

This shot was conducted 25 July, 1991 at 12:22 PDT using 31 kg of high explosives, and no Be The average wind speed at 10m was 5.5 m/s. The variation of Richardson number vs. height is presented in Table 14. The atmosphere was characterized as mildly stable with little variation in stability up to 850 m.

Table 14: Height vs. Ri for shot TG1-17

Height (m)	Ri
0-843	0.163
76-230	0.163

Table 14: Height vs. Ri for shot TG1-17

Height (m)	Ri
230-533	0.163
533 -843	0.161
850-1000	0.286

Figure 21 shows the history of the rise vs time for both the model and experimental observations.

Shot 415-a

This shot was conducted on 15 Aug., 1991 at 14:48 PDT using 11.4 kg of high explosives. The average wind speed at the 10 m height was 2.5 m/s. Table 15 shows the variation of Richardson number with height. This table shows there are four layers present in the first 1000 m of the atmosphere. This experiment was conducted under unstable conditions which is no surprise as it was conducted in the afternoon in mid-August.

Table 15: Height vs. Ri for shot 415-a

Height (m)	Ri
0-76	-0.226
76-230	-0.028
230-533	-0.028
533-843	-0.029
850-1000	0.072

Figure 22 shows the history of the rise vs time for both the model and experimental observations

Shot 3127-a

This shot was conducted on 4 Sept., 1991 19:33 PDT using 6.4 kg of high explosive. The average wind speed at 10 m was 7.5 m/s.

Table 16: Height vs. Ri for shot 3127-a

Height (m)	Ri
0-76	0.849
76-230	0.109
230-533	0.058
533-843	0.077
850-1000	-0.189

Figure 23 shows the history of the rise vs time for both the model and experimental observations

Shot 3115-a

This shot was conducted 5 Nov., 1991 at 15:43 PST using 20 kg of high explosive. The wind speed at 10 m was 2.3 m/s. Table 17 presents the variation of Richardson number vs height showing four layers ranging from slightly unstable, neutral and slightly stable.

Table 17: Height vs. Ri for shot 3115-a

Height (m)	Ri
0-76	0.072
82-230	-0.11
230-533	0.02
533-843	0.134
850-1000	0.149

Figure 24 shows the history of the rise vs time for both the model and experimental observations

Shot 3113-c

This shot was conducted on 4 Dec., 1991 at 16:11 PST using 16.5 kg of explosive. The average wind speed at 10 m was 1.5 m/s. Table 18 shows about three distinct layers in the first 1000 m ranging from stable to neutral.

Table 18: Height vs. Ri for Shot 3113-c

Height (m)	Ri
0-76	0.144
76-230	0.143
230-533	0.287
533-843	0.095
850-1000	0.007

Figure 25 shows the history of the rise vs time for both the model and experimental observations

4.2.2. Statistical analysis of the model predictions witht the experiments.

Table 19: Average absolute residual error of cloud top heights of model predictions and field observations for the Site 300 shots

Experiment Name	AARE
Shot 413-A	0.081
Shot TG1-17	0.149
Shot 415-A	0.099
Shot 3127-A	0.171
Shot 3115-A	0.181
Shot 3113-C	0.182

The average AARE for these shots is 0.141, with most of the error arising at the early times.

5.0. Correlation of Parameters Among VariousExperiments

As stated previously, a very important parameter determining the eventual equilibrium puff cloud height is the TNT mass equivalent of the explosive. For a given atmospheric stability, the greater the explosive mass, the greater will be the time to achieve equilibrium and the higher will be the steady state height be. In general, the lower layers of the atmosphere can experience a wide range of Richardson numbers, but above the boundary layer whose height can also vary considerably, the atmosphere is rather stable.

The experiments against which this model was calibrated had TNT equivalent masses ranging between 6 - 1020 kg, and the maximum time for which measurements were taken was 300 seconds after the ignition time. Thus, the experimental data is far from ideal.

Nevertheless, an attempt was made to correlate the mass of the explosive to parameters multiplying the puff-atmospheric turbulence parameter, $\mathbf{k_{p\text{-}a}}$, and the effective cross-sectional area, Ξ, as functions of explosive mass and average Richardson number up to the boundary layer.

Denote constants, C_1 and C_2 as input constants that multiply $\mathbf{k_{p\text{-}a}}$, and Ξ. Since the most prevalent TNT mass in the Roller Coaster series was 63.6 kg of TNT, correlations of TNT mass, denoted by M were made.

Neutrally Stable Atmosphere::

C_1 0.40 (89)

$C_2 = 0.5$ (90)

Mildly Stable Atmosphere:

$C_1 = 0.5 - 0.15 \log_{10}(M/63.6)$ (91)

$C_2 = 0.6$ (92)

Very Stable Atmosphere:

$C_1 = 0.6 - 0.34 \log_{10}(M/63.6)$ (93)

$C_2 = 0.6 + 0.094 \log_{10}(M/63.6)$ (94)

Unstable Atmosphere with updrafts:

$C_1 = 0.19$ (95)

$C_2 = 0.37$ (96)

For the constants, C_1 and C_2, in Eqs(91-94), a minimum value of C_1 and C_2 , given by Eq(95) and Eq(96), respectively should be used. Because the model was calibrated with a limited set of experiments, extrapolation to explosive masses beyond the calibration limits will most likely be unreliable. For this reason, it is recommended that a family of history curves for the height and cloud major and minor axes be generated to bracket these parameters.

6.0 Relation of this model to a particle dispersion model

This model of buoyant explosive puffs is the basis for a hazardous contaminated particle dispersion model that will couple to the LLNL code called LODI. At every time step, this model outputs the height of the puff center, z, the dimensions of the cloud cap, (r, h^+, and h^-), the density of the puff, the velocity components, w_p and u_p, and the down wind trajectory of the puff center, assuming the puff center is advected by the ambient wind at the height, z. The particle diffusion is assumed to be proportional to the cap-cloud dimensions. Particles will be deleted from consideration if they wander outside the dimensions of the cloud cap.

7.0. Summary

A buoyant puff rise model was developed from the strong conservative form of the Navier-Stokes equations by integrating over all space to yield a set of coupled nonlinear ODEs dependent upon the discontinuity of mass, momentum, and energy at the puff-atmosphere interface. The puff cloud was allowed to evolve from a sphere to an ellipsoid. It was found that the rise history of an explosive cloud depended upon not only the explosive mass and temperature, but also upon the strength of the puff-atmospheric turbulence, the wind speed, and the effective cross-sectional areas. The coupled nonlinear Ordinary Differential Equations (ODEs) represented in the model are integrated in a matter of a few seconds of computer time.

The buoyant rising forces of the hot ellipsoidal puff are dissipated by radiation, entrainment from the mean flow, puff-atmospheric turbulence, and the ambient turbulence. From model experimentation, the ambient and puff-atmospheric turbulence were observed to affect the rate at which a puff cloud rises. From the limited number of model comparisons to field experiments, the model produced good agreement with actual puff rise histories.

It is observed that slugs of hot gas has its own turbulence properties as the slug rises in the ambient atmosphere. The atmosphere is very turbulent in the unstable (Ri <0) region, the puff-atmosphere turbulence diffusivities are quite small. In the very stable atmospheres (Ri > 1), the atmospheric diffusivities are ineligible, but the puff-atmosphere turbulence diffusivities are quite large. It would be very desirable to obtain a better understanding of this phenomenon to better enhance this model.

8.0. Acknowledgements

This work was performed under the auspicies of the U.S. Department of Energy by Lawrence Livermore National Laboratory under Contract No. W-7405-Eng.48

9.0 References

Baker,W.E., Cox, P.A. Westine, P.S., Kulesz, J.J, and Strehlow, R.A. (1983), "Explosion Hazards and Evaluation", Elsevier Scientific Publ. Co, NY.

Baskett, R. A. and Fries, R.P. (1997), "Measurement and dispersion modeling of beryllium from high explosive tests at Site 300 during 1991", LLNL, UCRL

Boughton, B.A. and DeLaurentis (1987) "An integral model of plume rise from high explosive detonations", vol. 70, pp 27-32. ASME-HTD 24th Annual National Heat Transfer Conference.

Church, H.W, (1968) "Cloud Rise from High Explosive Detonations," SC-RR-68-903, Sandia National Laboratory.

Daly, J.W. and Harleman, D.R.F (1966), " Fluid Dynamics", Addison-Wesley Publ. Reading, MA.

Ermak, D.L. (1990), "User's manual for SLAB: An atmospheric dispersion model for denser-than-air releases", UCRL-MA-105607, Lawrence Livermore National Laboratory.

Fleagle, R.G. and Businger, J.A. (1980) "An Introduction to Atmospheric Physics", Academic Press, Inc. NY.

Libby, P.A. and Willliams, F.A. (1980), Turbulent Reacting Flows, Springer Verlag, Berlin; New York.

Pielke, R.A. (1984), "Mesoscale Meteorological Modeling, Academic Press, New York.

Stull, R.B. (1988) "An Introduction to Boundary Layer Meteorology", Kluwer Academic Publ., Dordrecht, Netherlands.

Turner, J.S. (1973) "Buoyancy Effects in Fluids", Cambridge University Press.

Whitham, G.B. (1974) "Linear and nonlinear Waves", John Wiley and Sons, NY.

Zhang, X.J., Moussa, N.A.,Groszmann, D.E., Beach, A.B. and Noland,R.B (1995) "A Simple Analytical Buoyant Puff Rise Model", Manuscript.

10. List of Figures

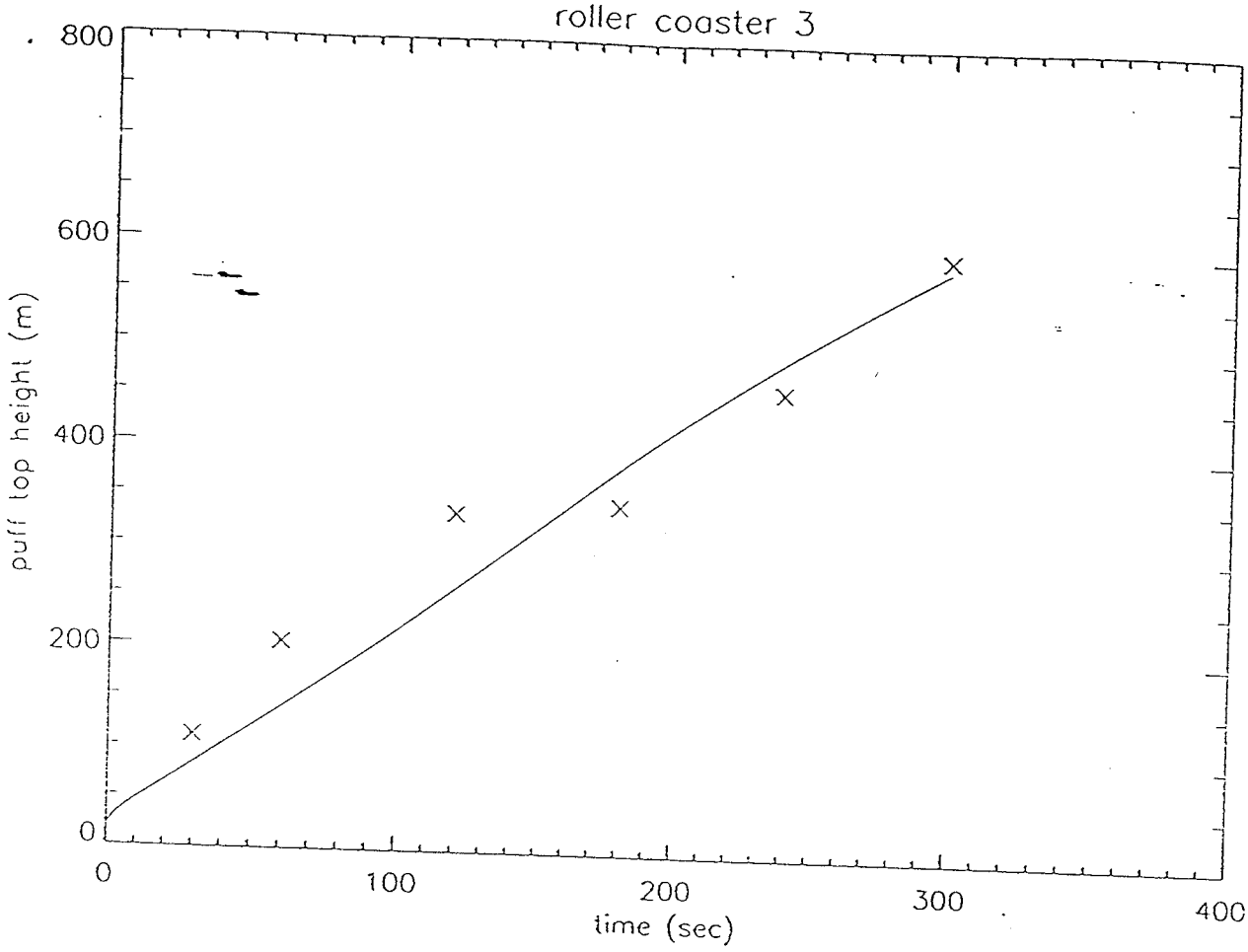

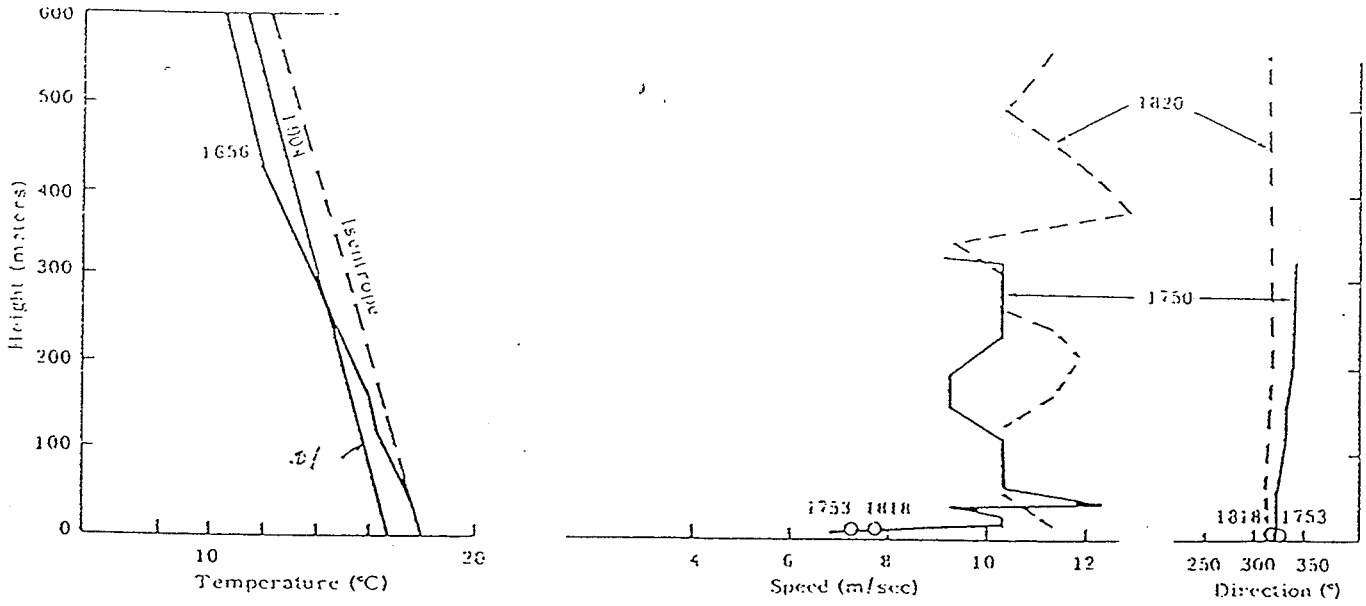

Figure A-2. HE Shot No. 2, 1753 PDT, 140 Pounds;
HE Shot No. 3, 1818 PDT, 140 Pounds

Figure 4. Height history for the Roller Coaster 3 experiment in a neutral atmosphere.

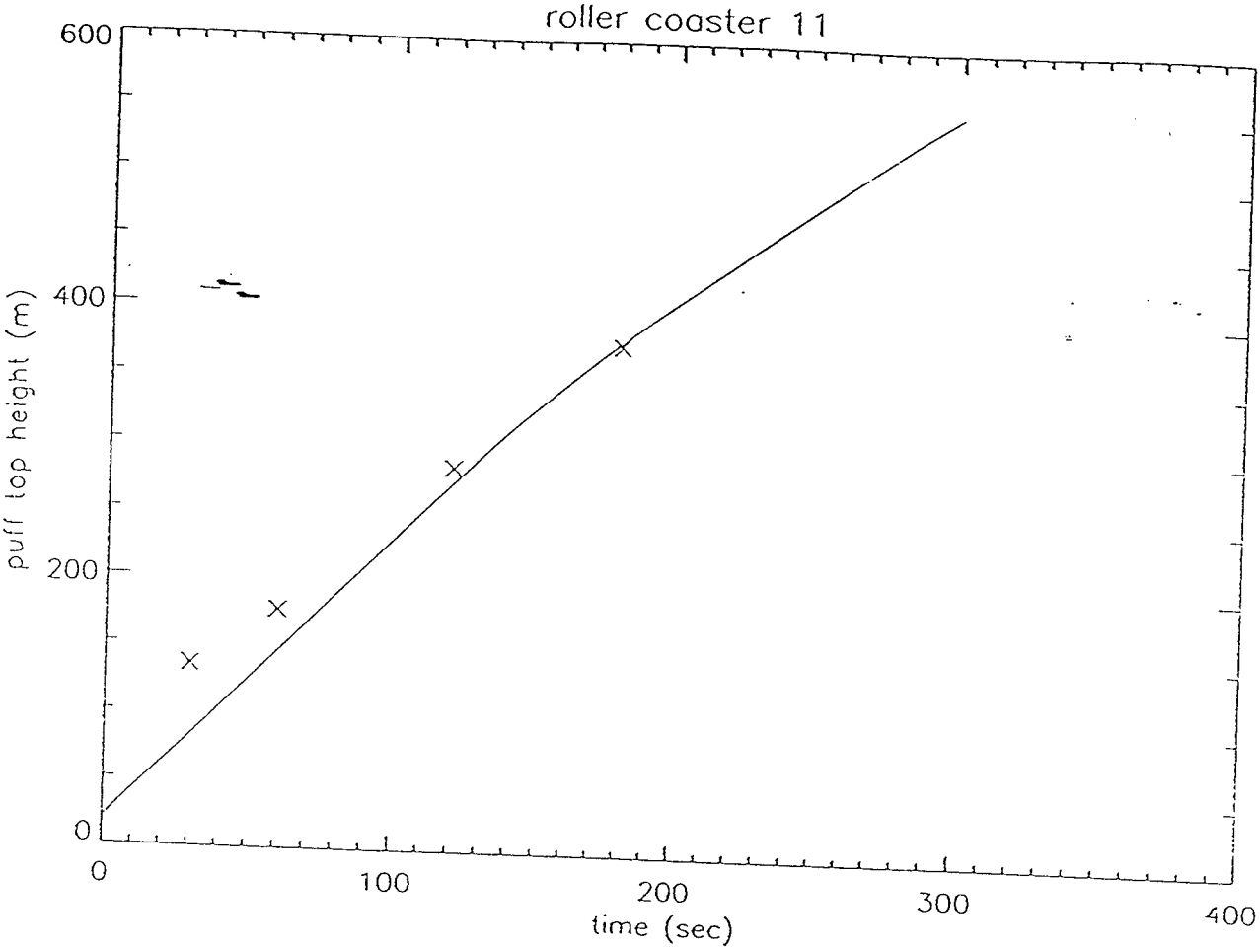

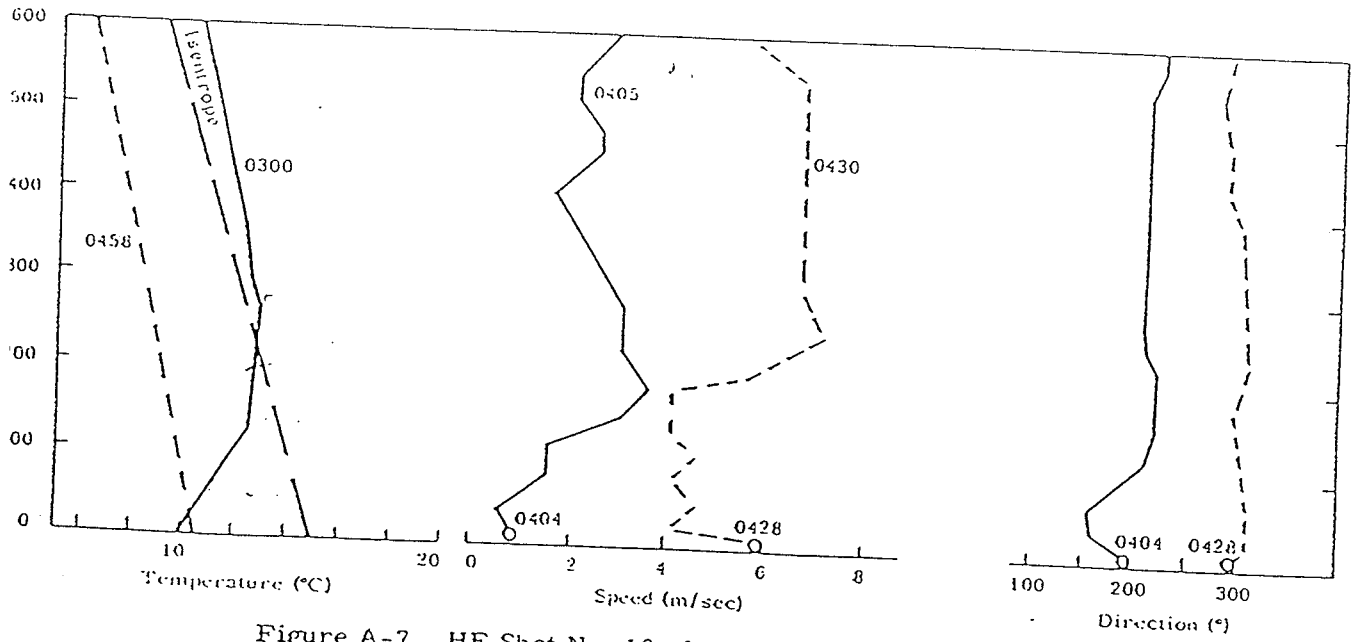

Figure A-7. HE Shot No. 10, 0404 PDT, 420 Pounds;
HE Shot No. 11, 0428 PDT, 140 Pounds

Figure 5. Height history for the Roller Coaster 11 experiment in a neutral atmosphere.

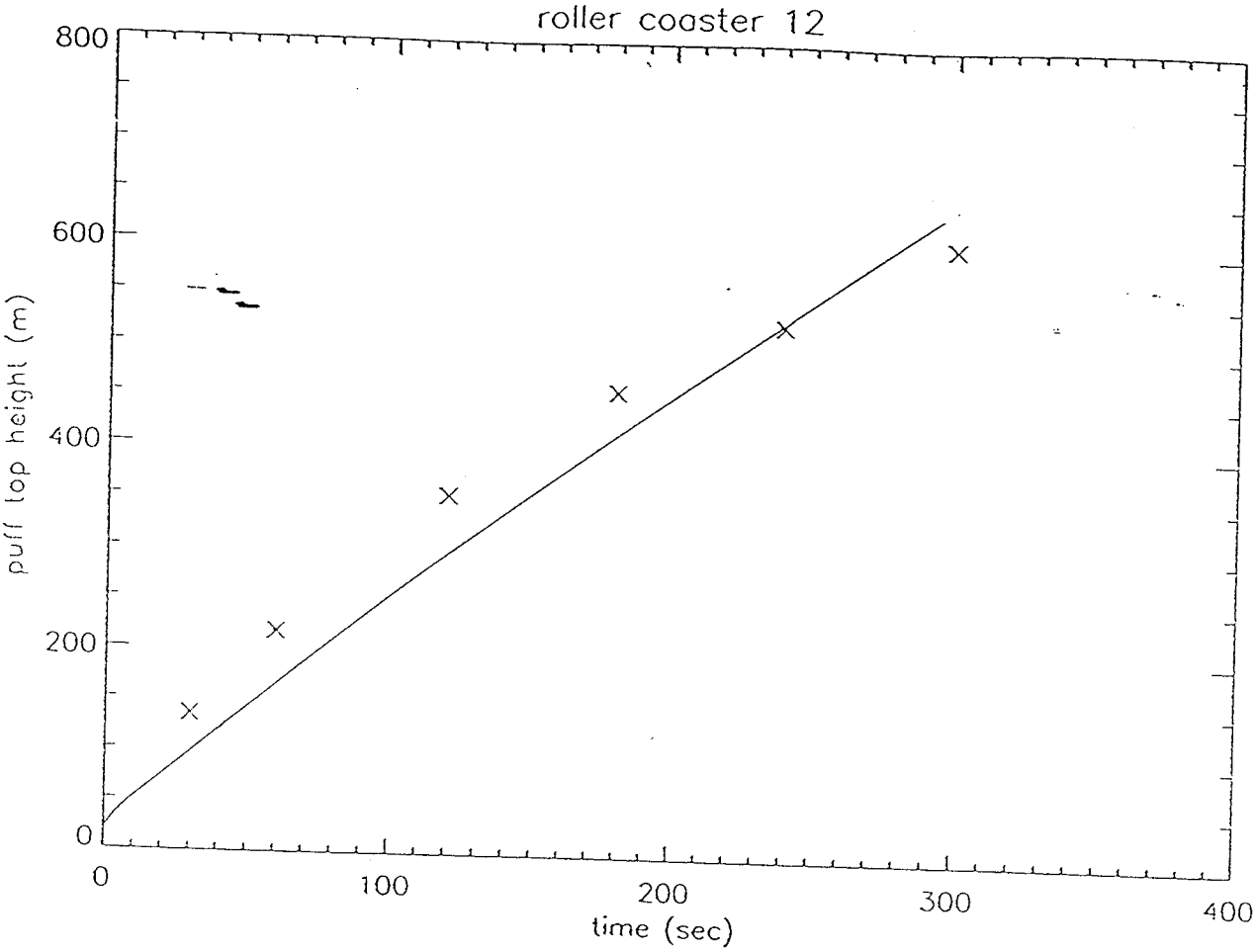

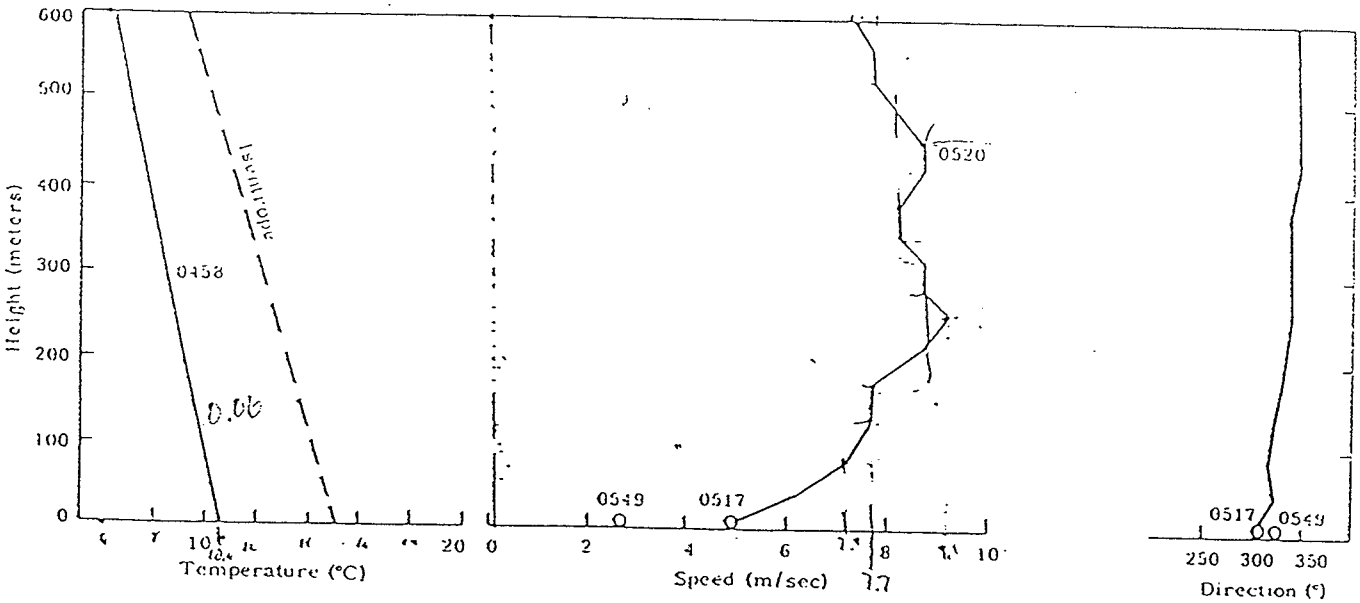

Figure A-8. HE Shot No. 12, 0517 PDT, 140 Pounds;
HE Shot No. 13, 0549 PDT, 560 Pounds

Figure 6. Height history for the Roller Coaster 12 experiment in a neutral atmosphere.

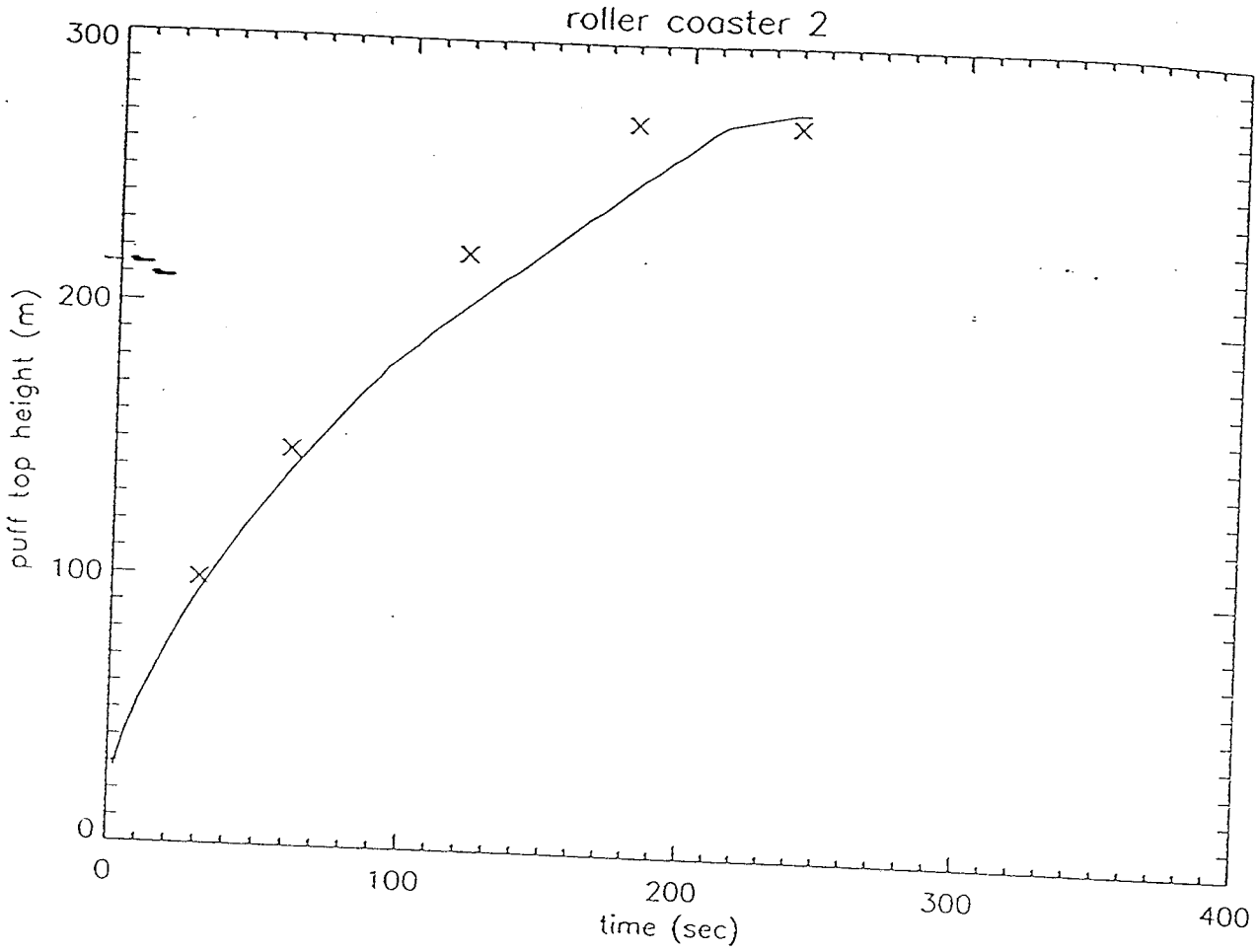

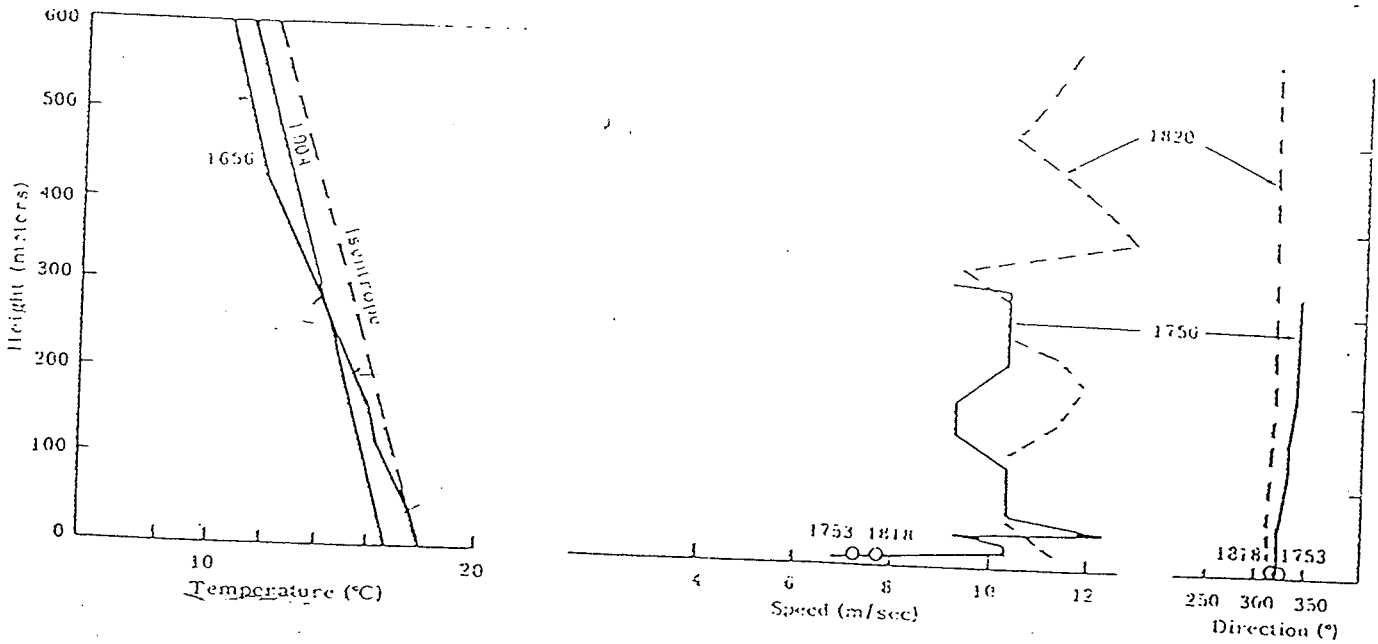

Figure A-2. HE Shot No. 2, 1753 PDT, 140 Pounds;
HE Shot No. 3, 1818 PDT, 140 Pounds

Figure 7. Height history for the Roller Coaster 2 experiment in a mildy stable atmosphere.

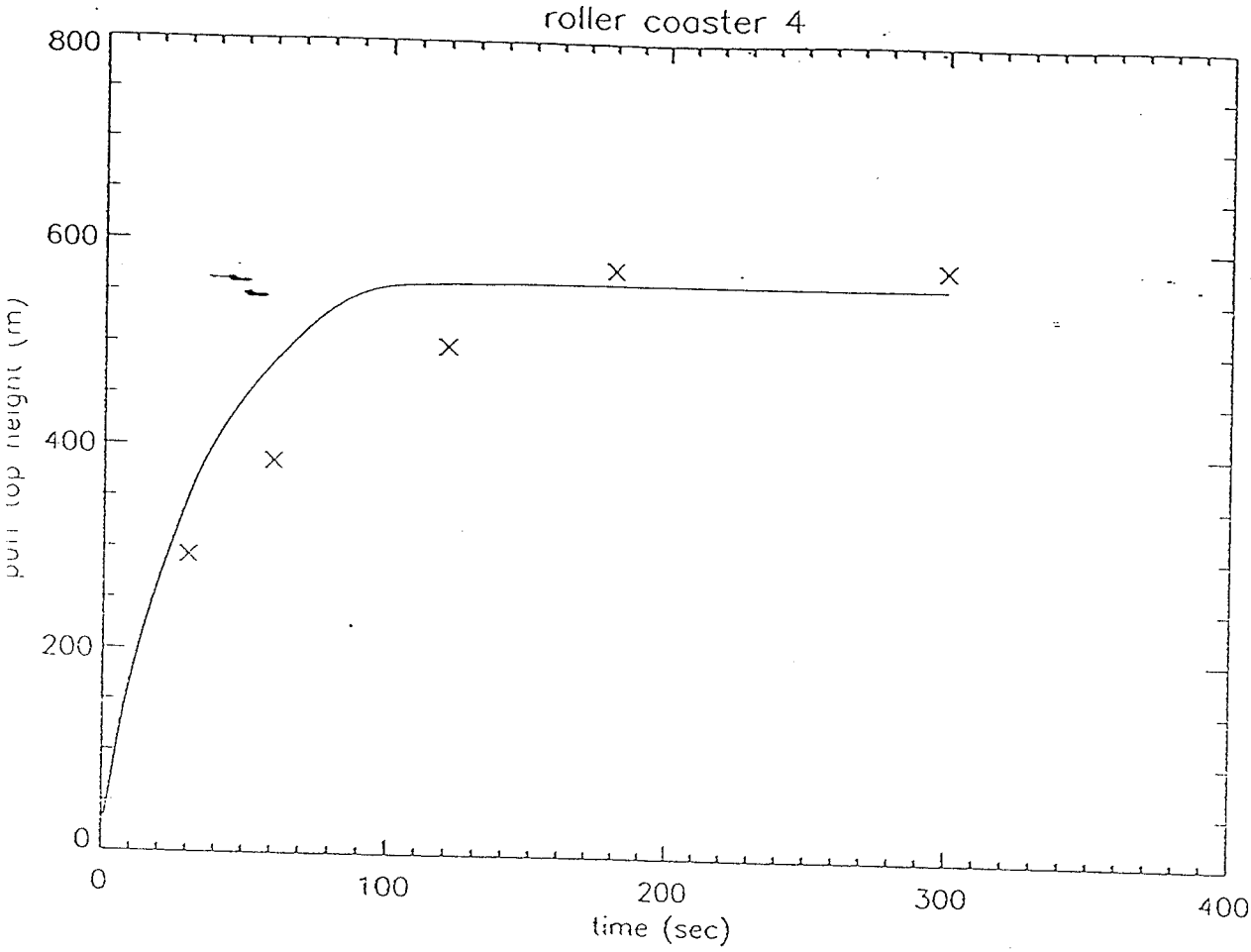

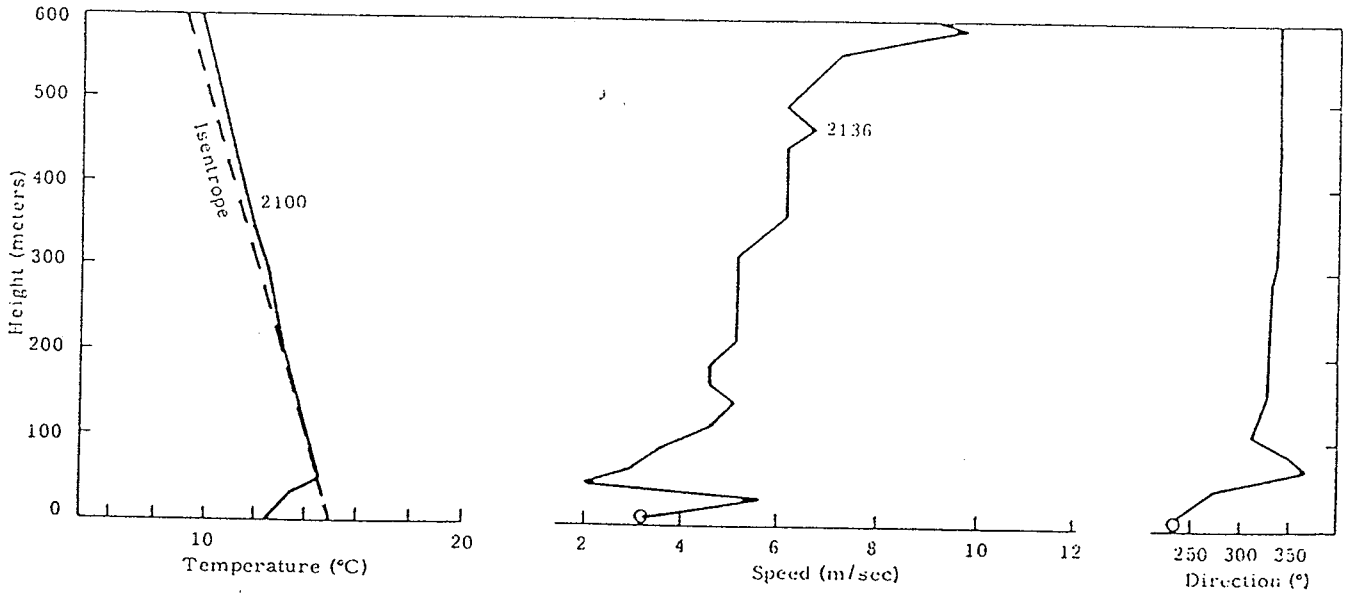

Figure A-3. HE Shot No. 4, 2150 PDT, 1600 Pounds

Figure 8. Height history for the Roller Coaster 4 experiment in a mildy stable atmosphere.

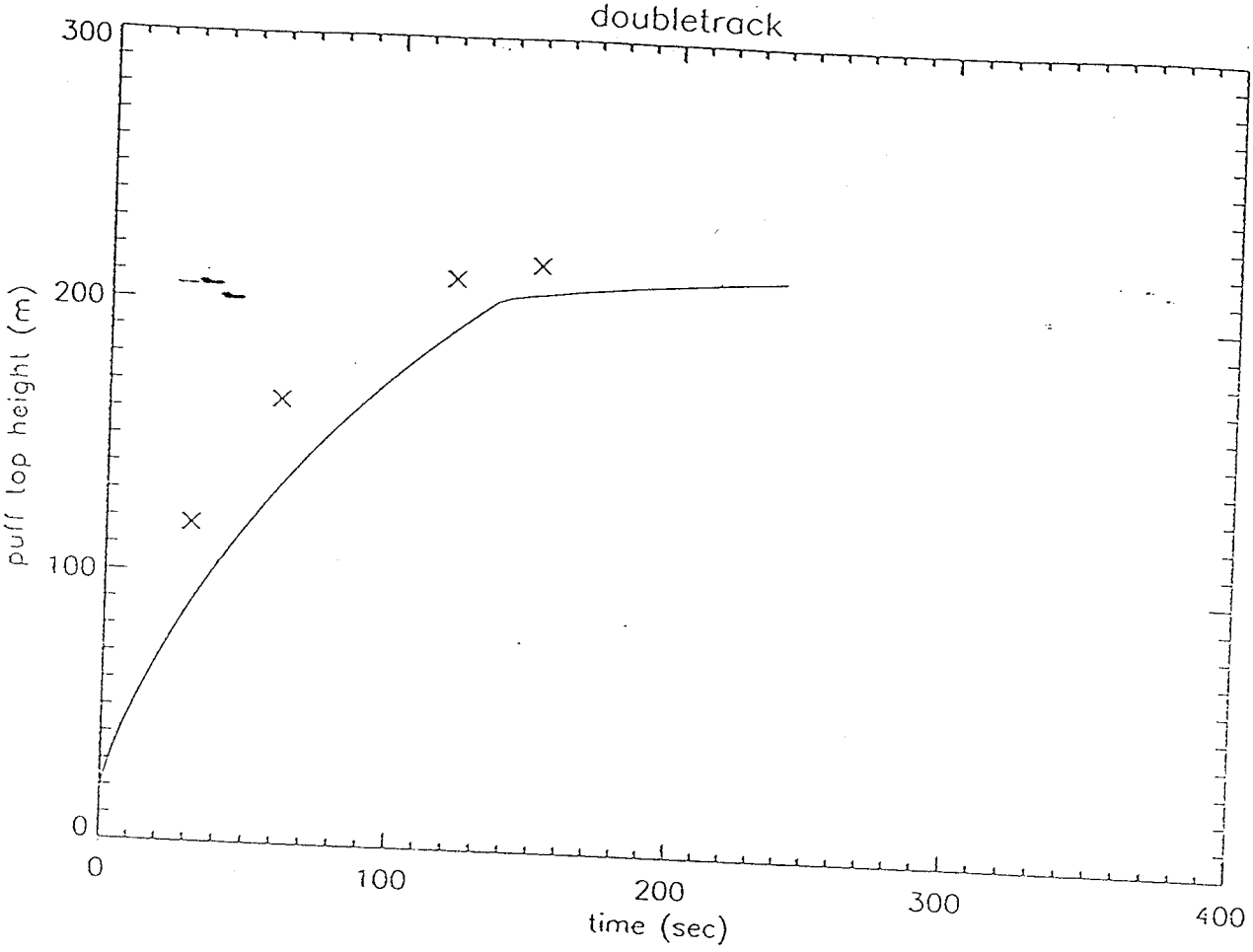

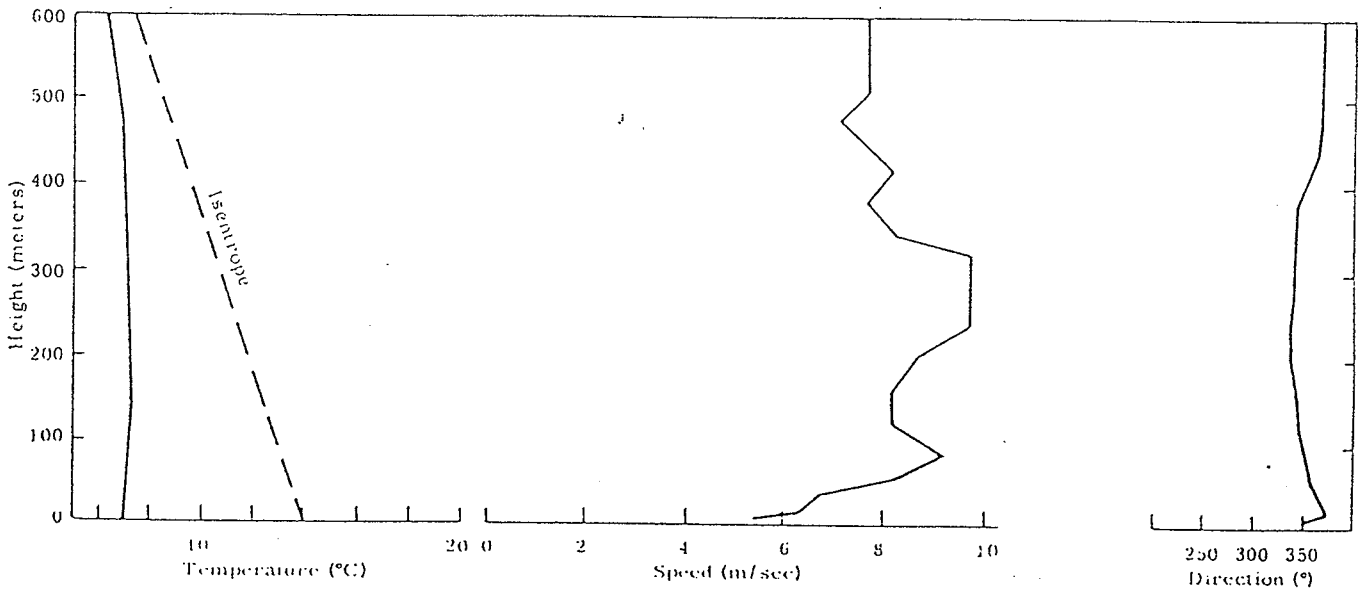

Figure A-9. Double Tracks, 0255 PDT, 118 Pounds

Figure I0. Height history for the Double Track experiment in a mildy stable atmosphere.

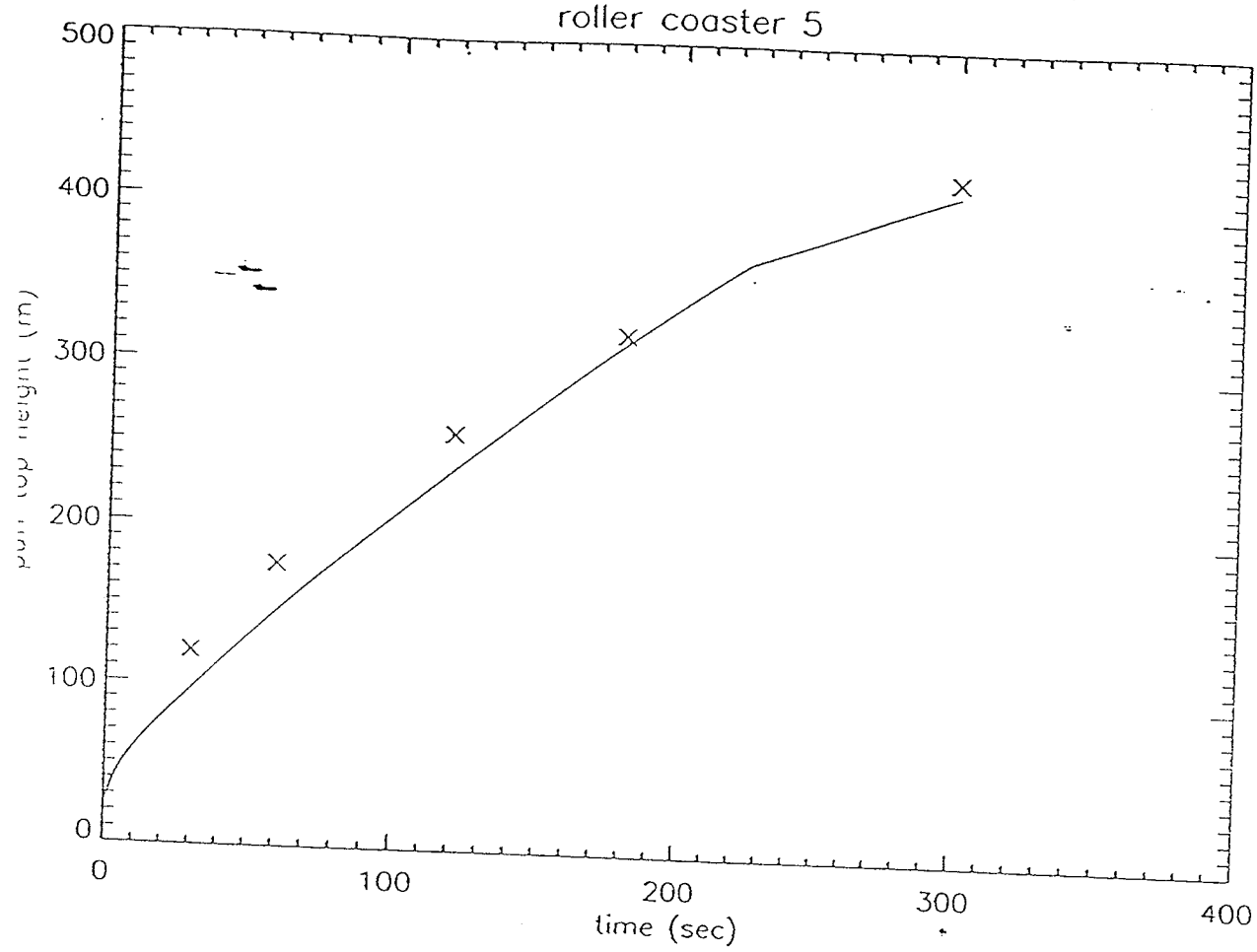

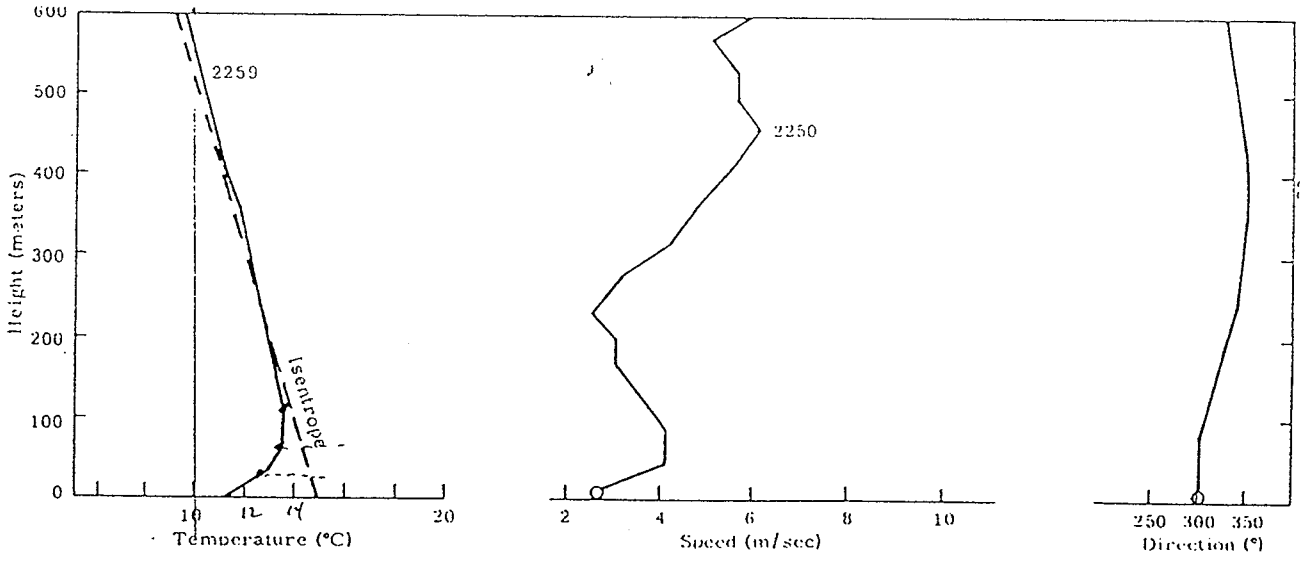

Figure A-4. HE Shot No. 5, 2248 PDT, 140 Pounds

Figure 11. Height history for the Roller Coaster 5 experiment in a very stable atmosphere.

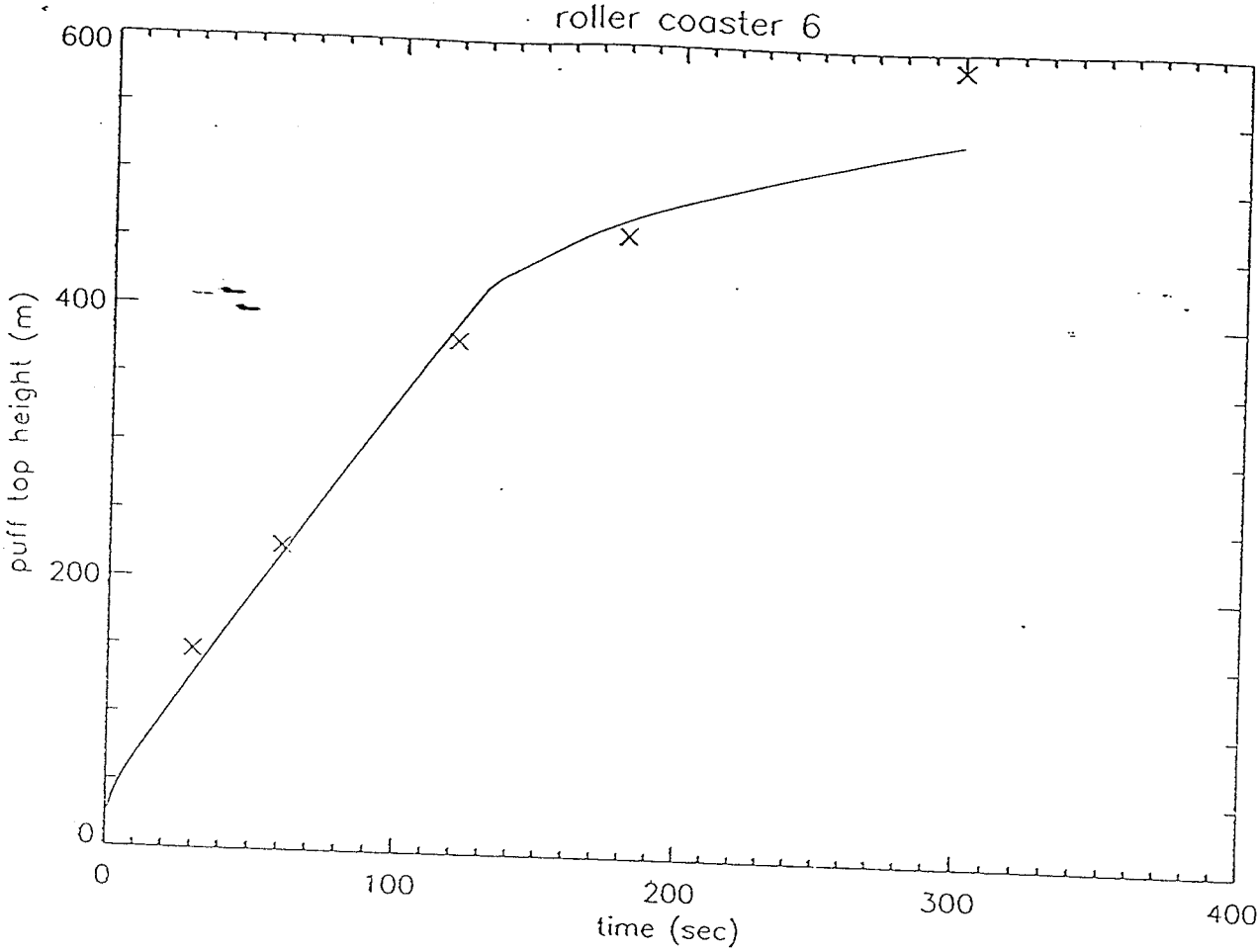

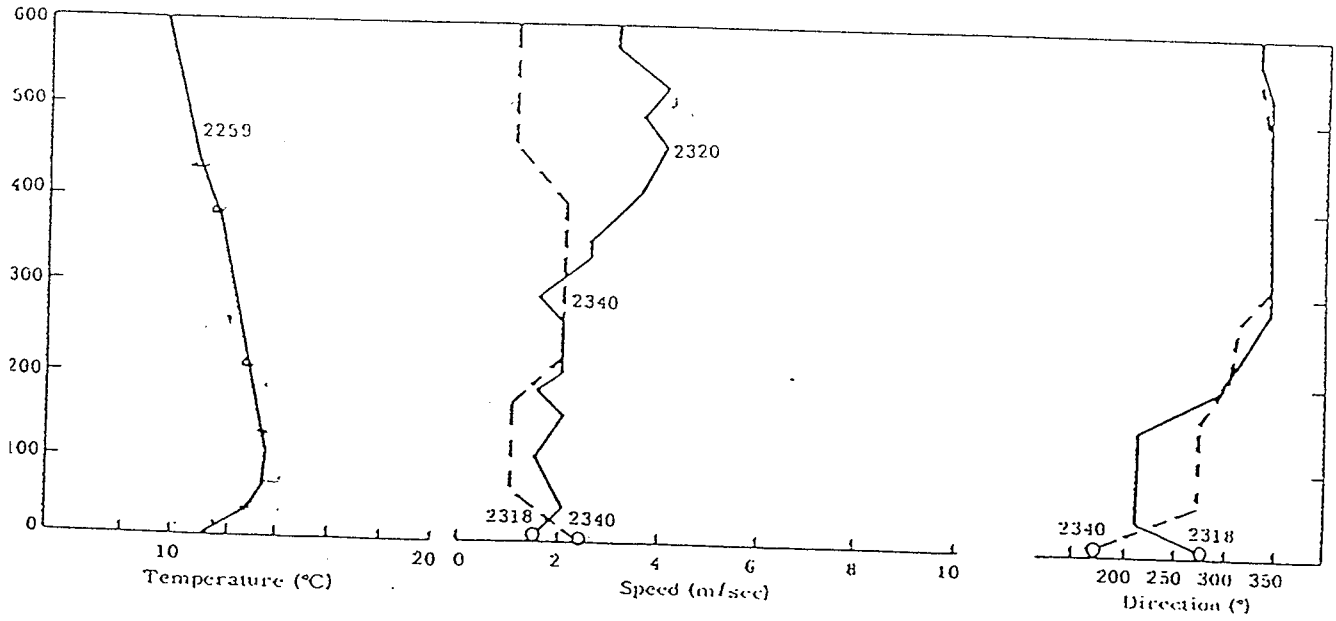

Figure A-5. HE Shot No. 6, 2318 PDT, 560 Pounds;
HE Shot No. 7, 2340 PDT, 140 Pounds

Figure 12. Height history for the Roller Coaster 6 experiment in a very stable atmosphere.

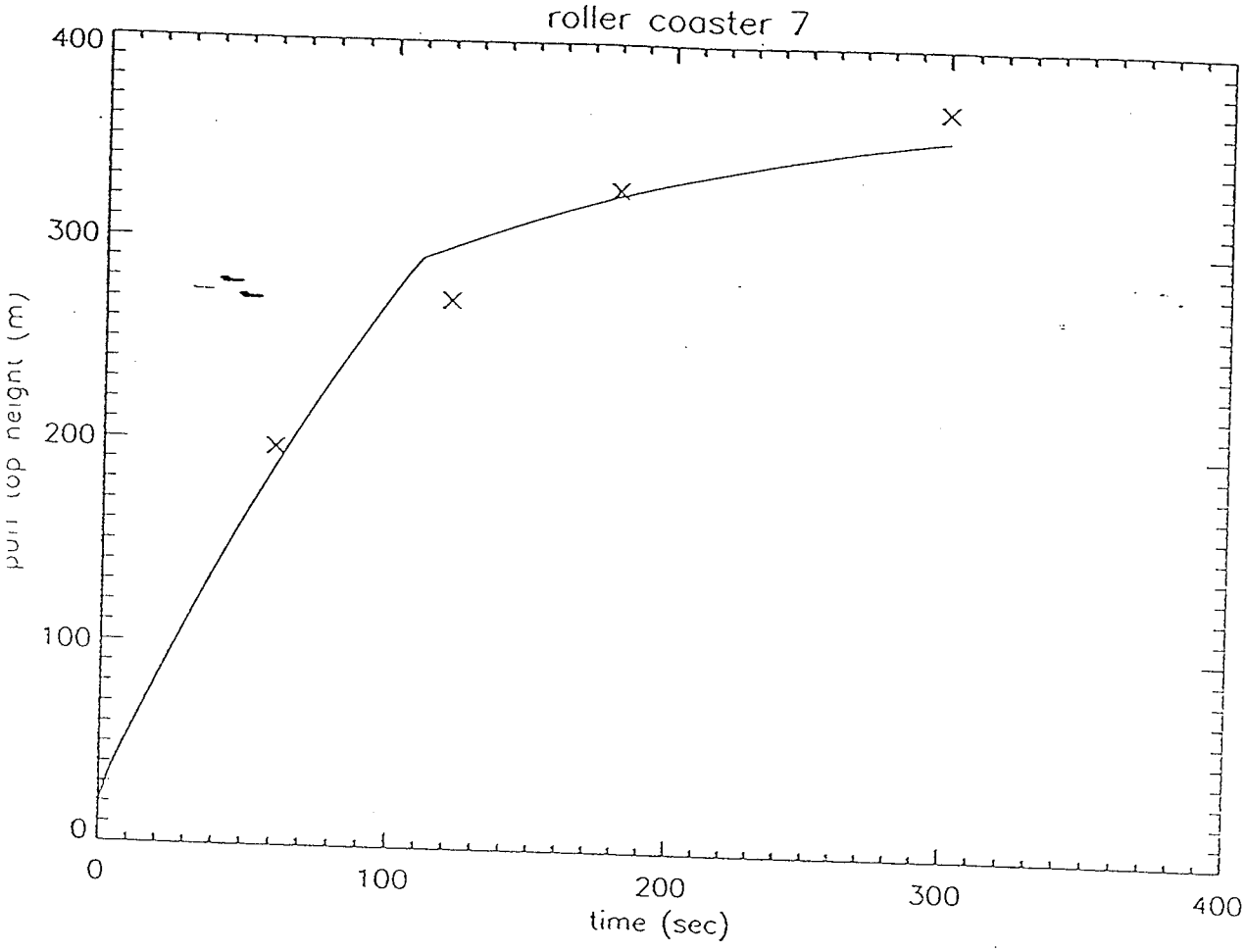

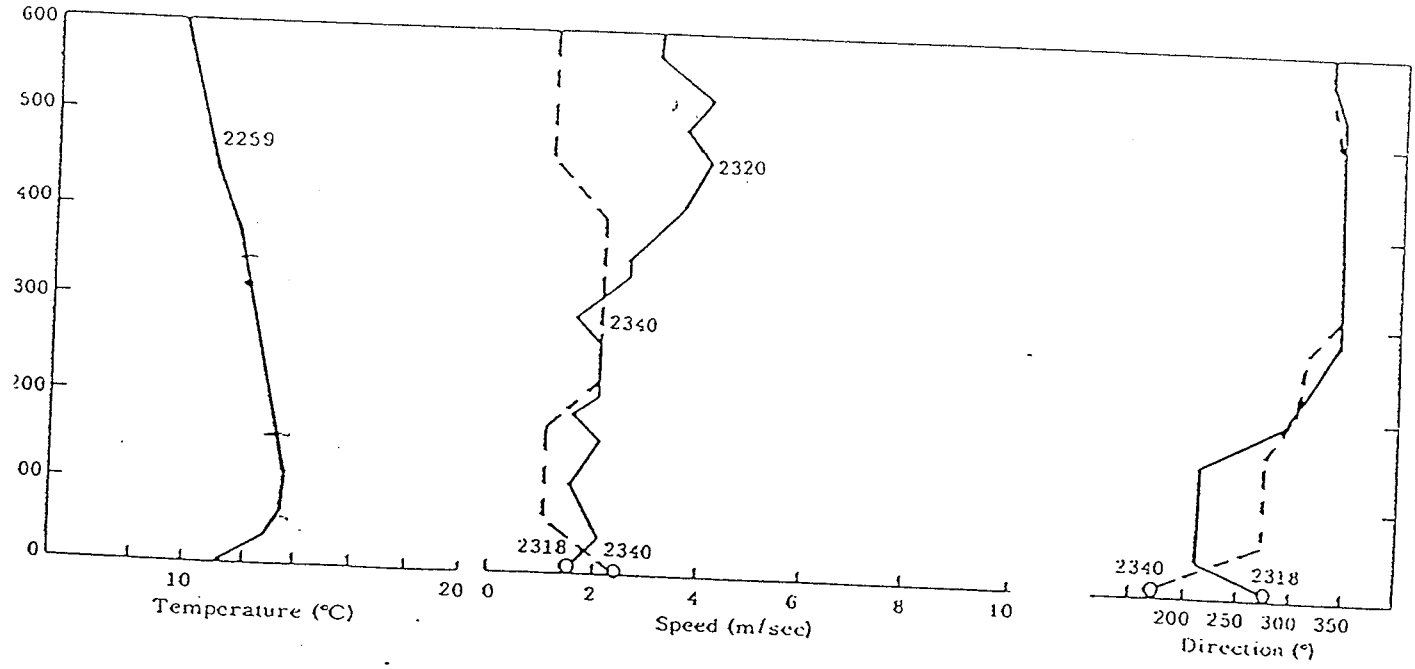

Figure A-5. HE Shot No. 6, 2318 PDT, 560 Pounds;
HE Shot No. 7, 2340 PDT, 140 Pounds

Figure 13. Height history for the Roller Coaster 7 experiment in a very stable atmosphere.

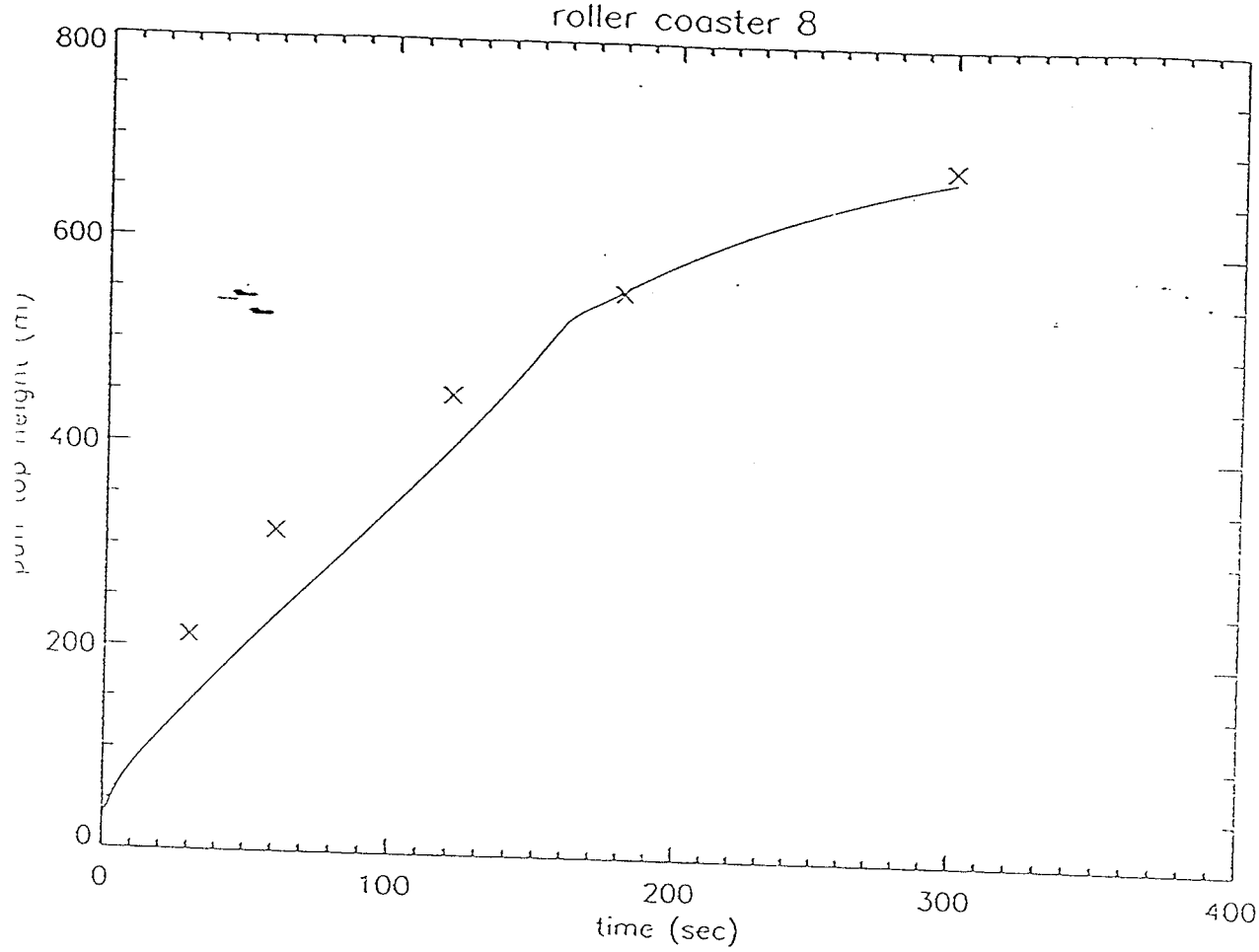

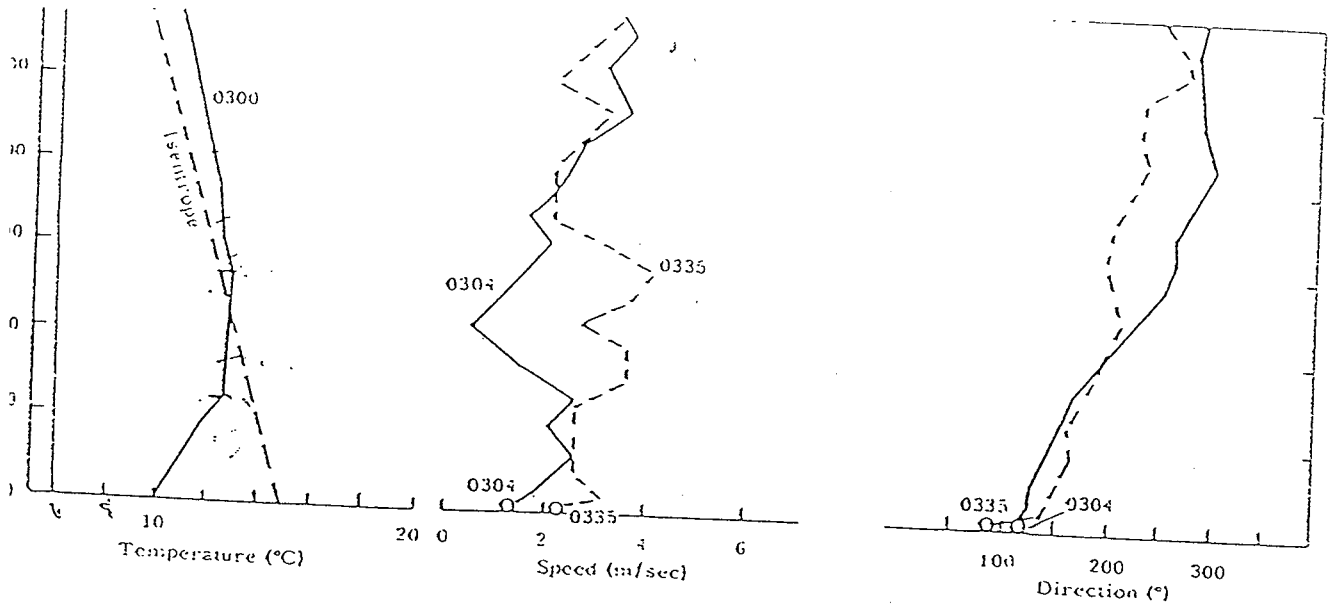

Figure A-6. HE Shot No. 8, 0304 PDT, 1600 Pounds;
HE Shot No. 9, 0335 PDT, 140 Pounds

Figure 14. Height history for the Roller Coaster 8 experiment in a very stable atmosphere.

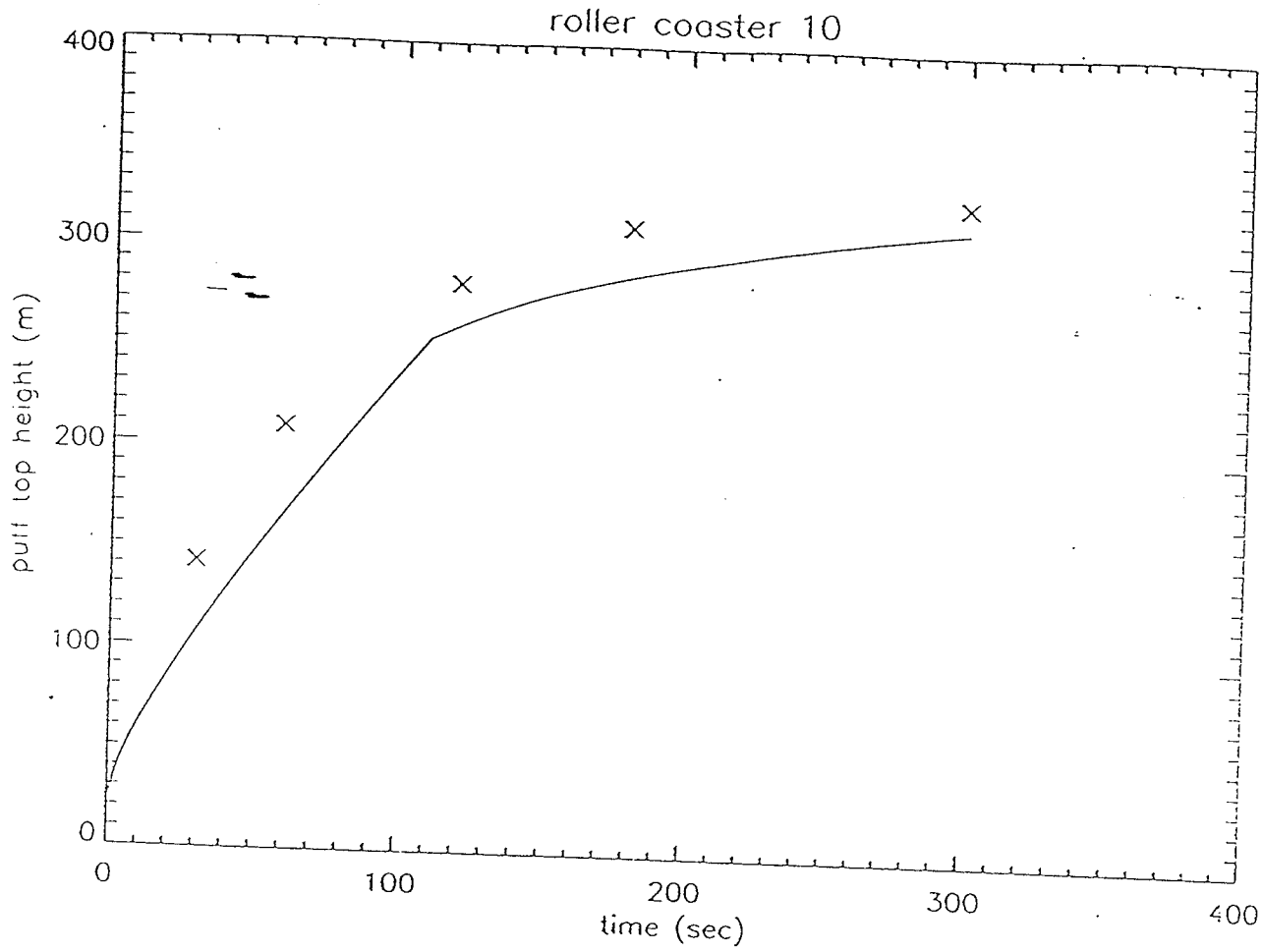

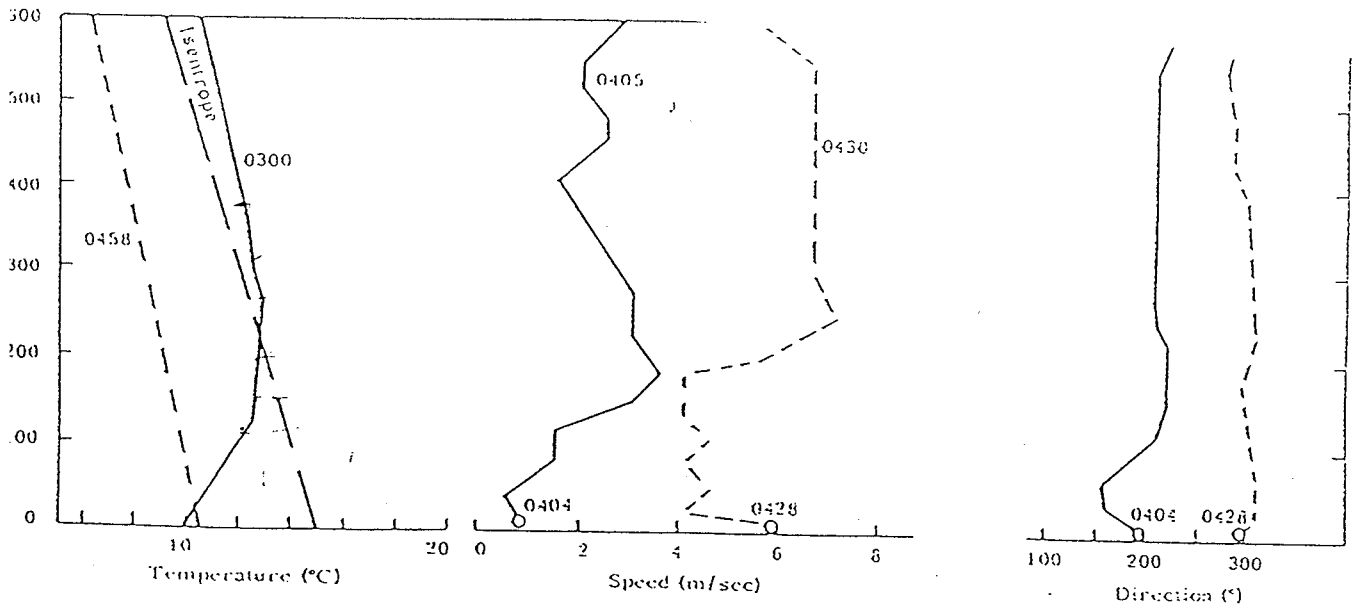

Figure A-7. HE Shot No. 10, 0404 PDT, 420 Pounds;
HE Shot No. 11, 0428 PDT, 140 Pounds

Figure 15. Height history for the Roller Coaster 10 experiment in a very stable atmosphere.

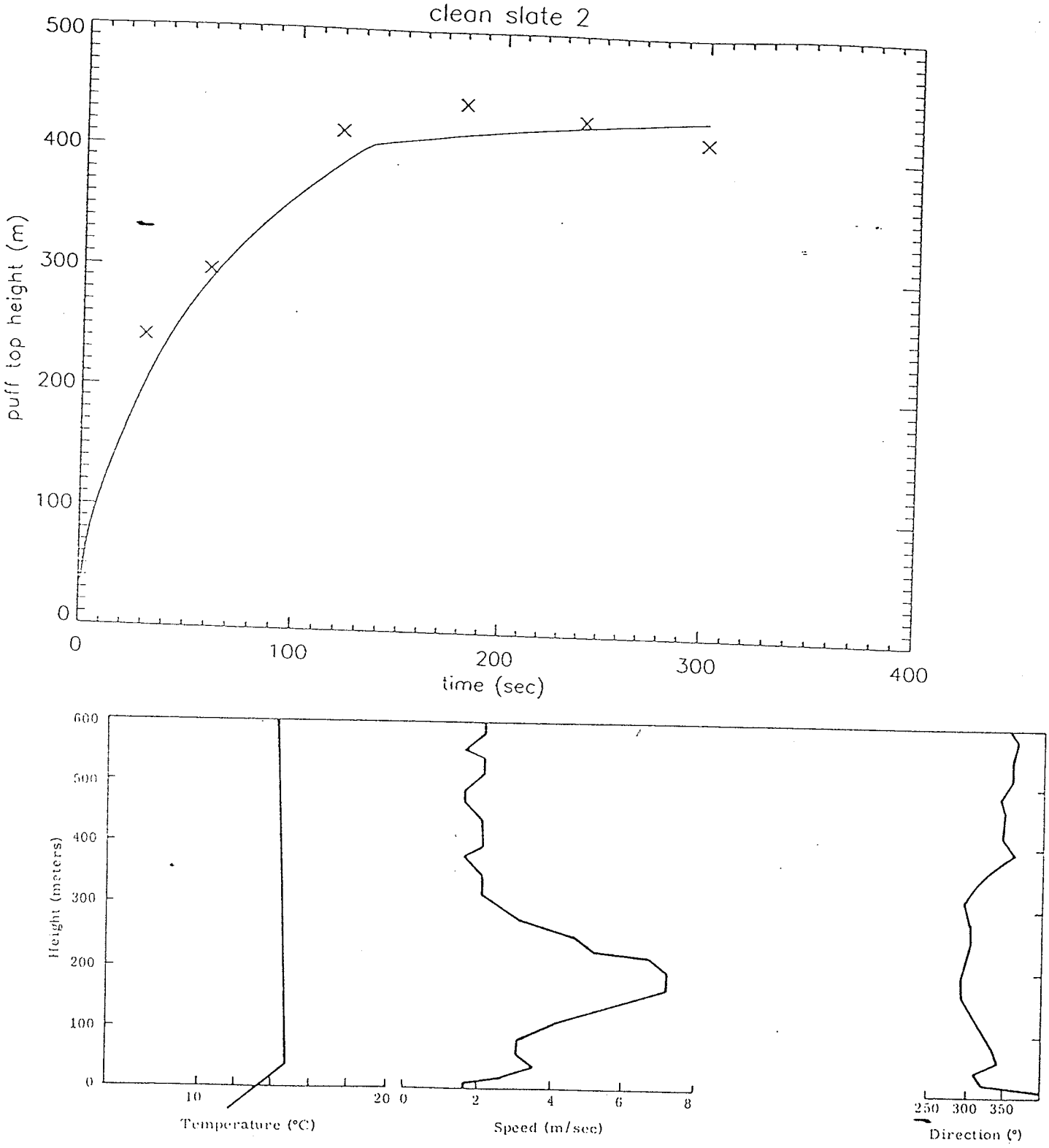

Figure A-11. Clean Slate 2, 0347 PDT, 2242 Pounds

Figure 16. Height history for the Clean Slate 2 experiment in a very stable atmosphere.

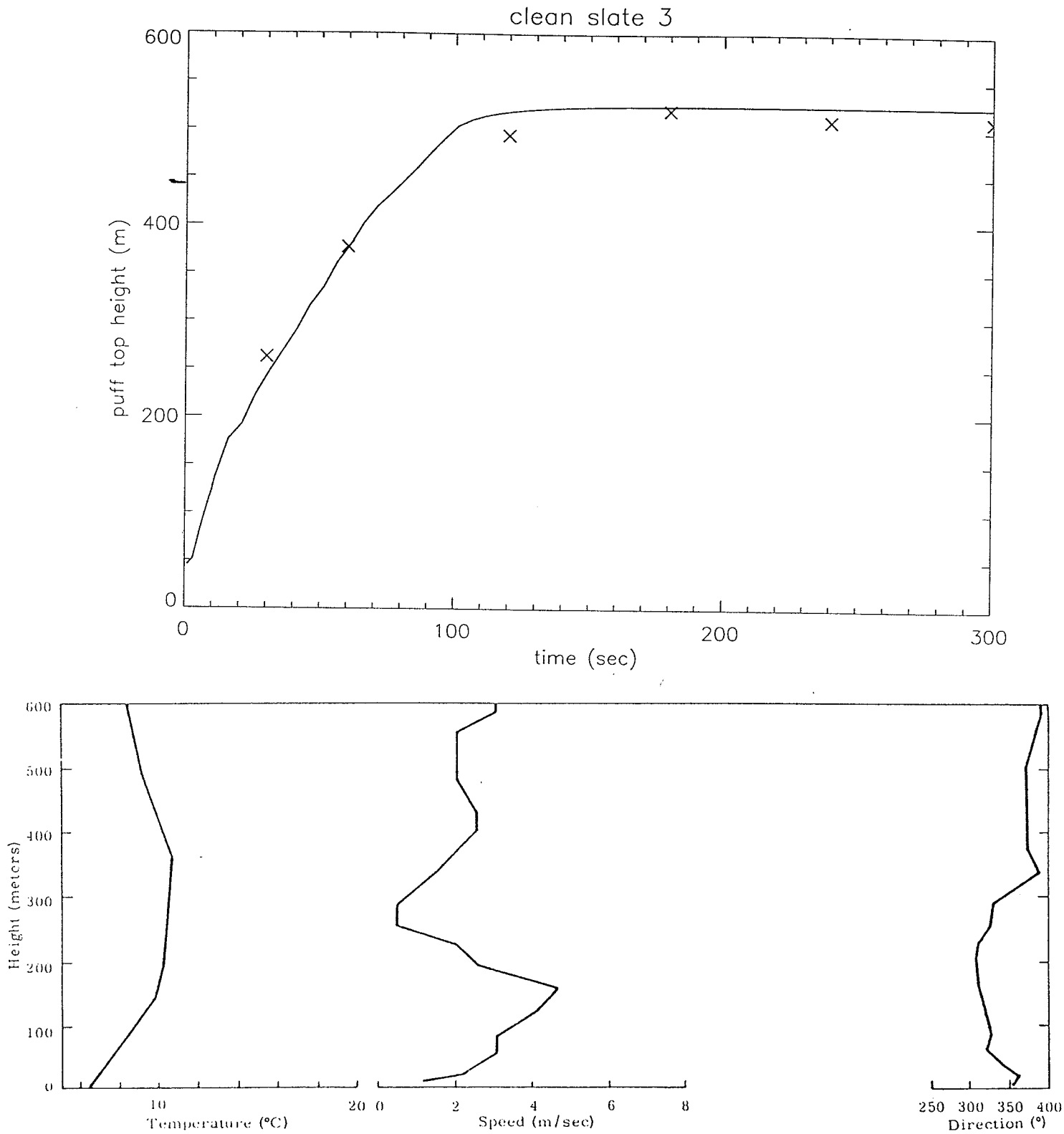

Figure A-12. Clean Slate 3, 0330 PDT, 2242 Pounds

Figure 17. Height history for the Clean Slate 3 experiment in a very stable atmosphere.

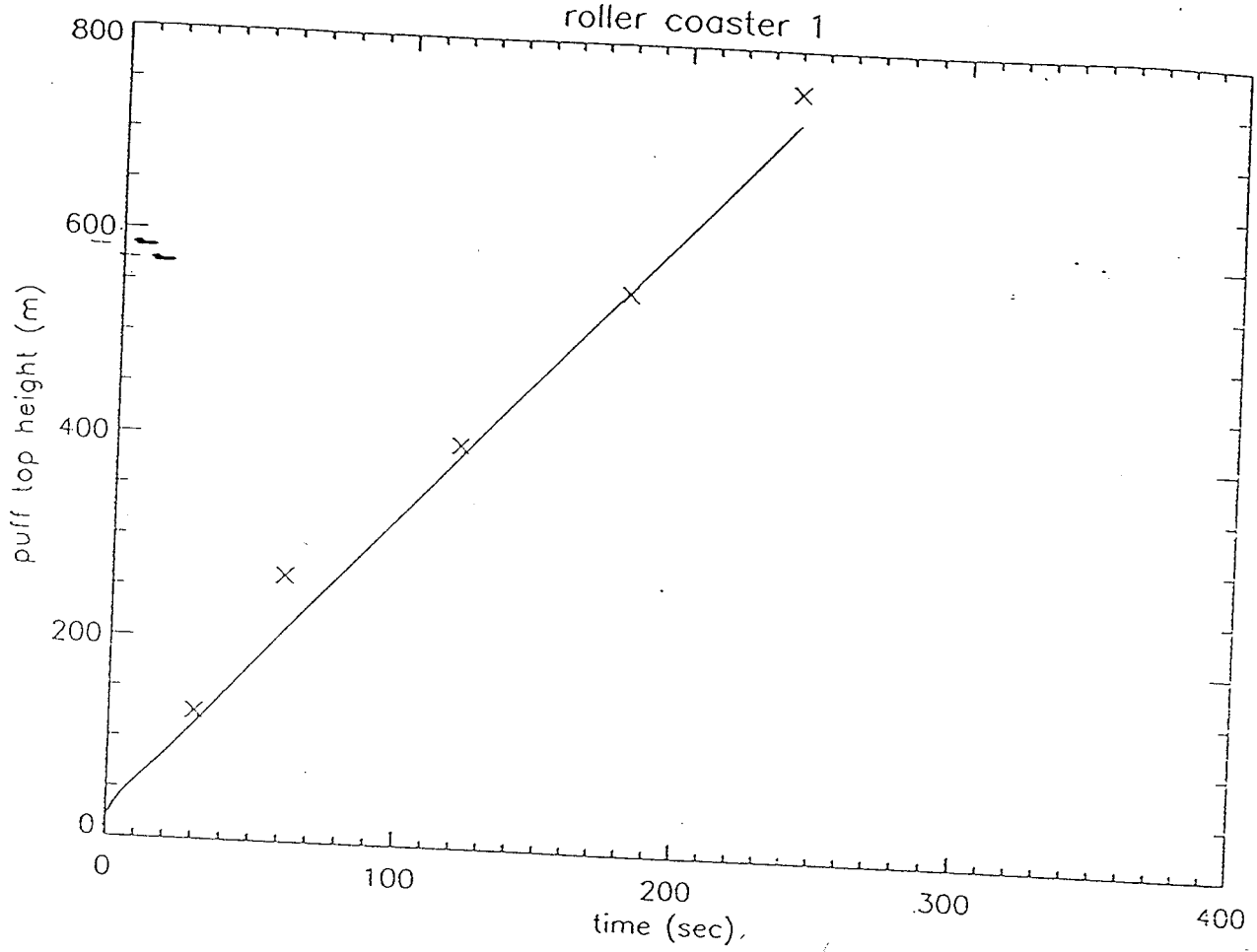

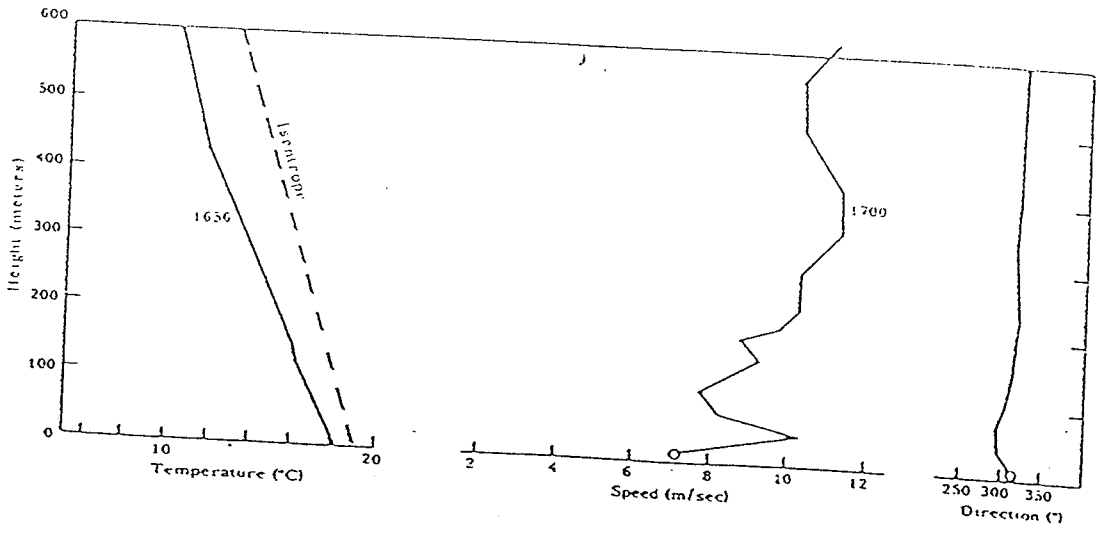

Figure A-1. HE Shot No. 1, 1720 PDT, 140 Pounds

Figure 18. Height history for the Roller Coaster 1 experiment in an unstable atmosphere.

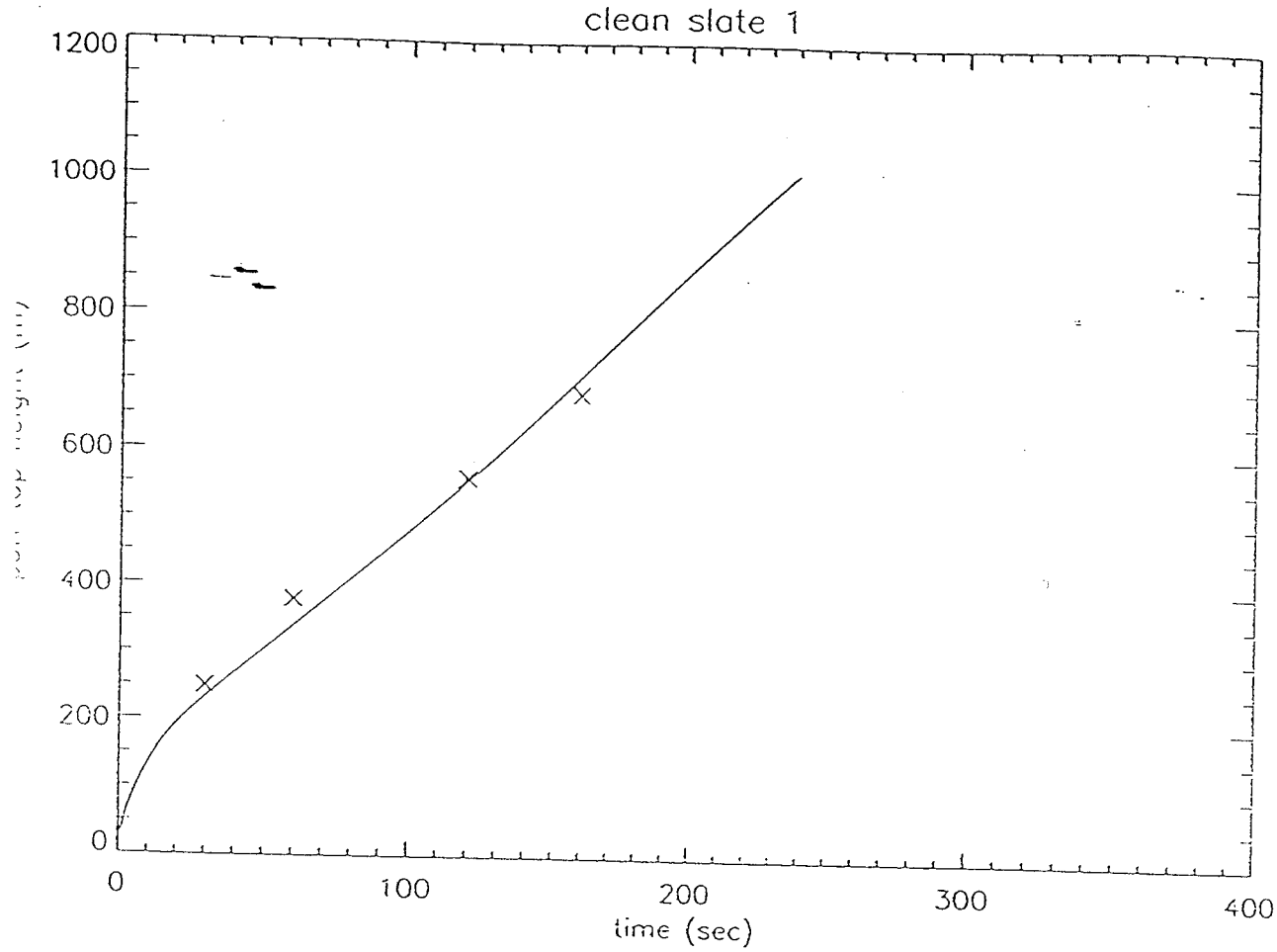

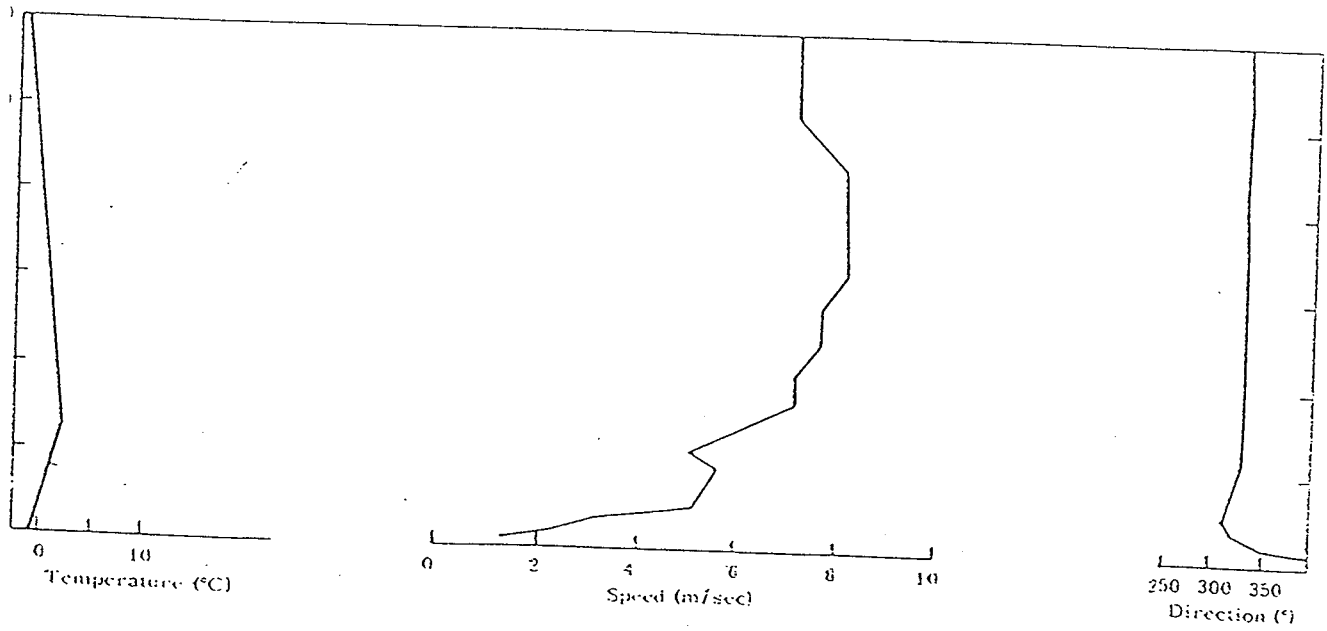

Figure A-10. Clean Slate 1, 0415 PDT, 1062 Pounds

Figure 19. Height history for the Clean Slate 1 experiment in an unstable atmosphere.

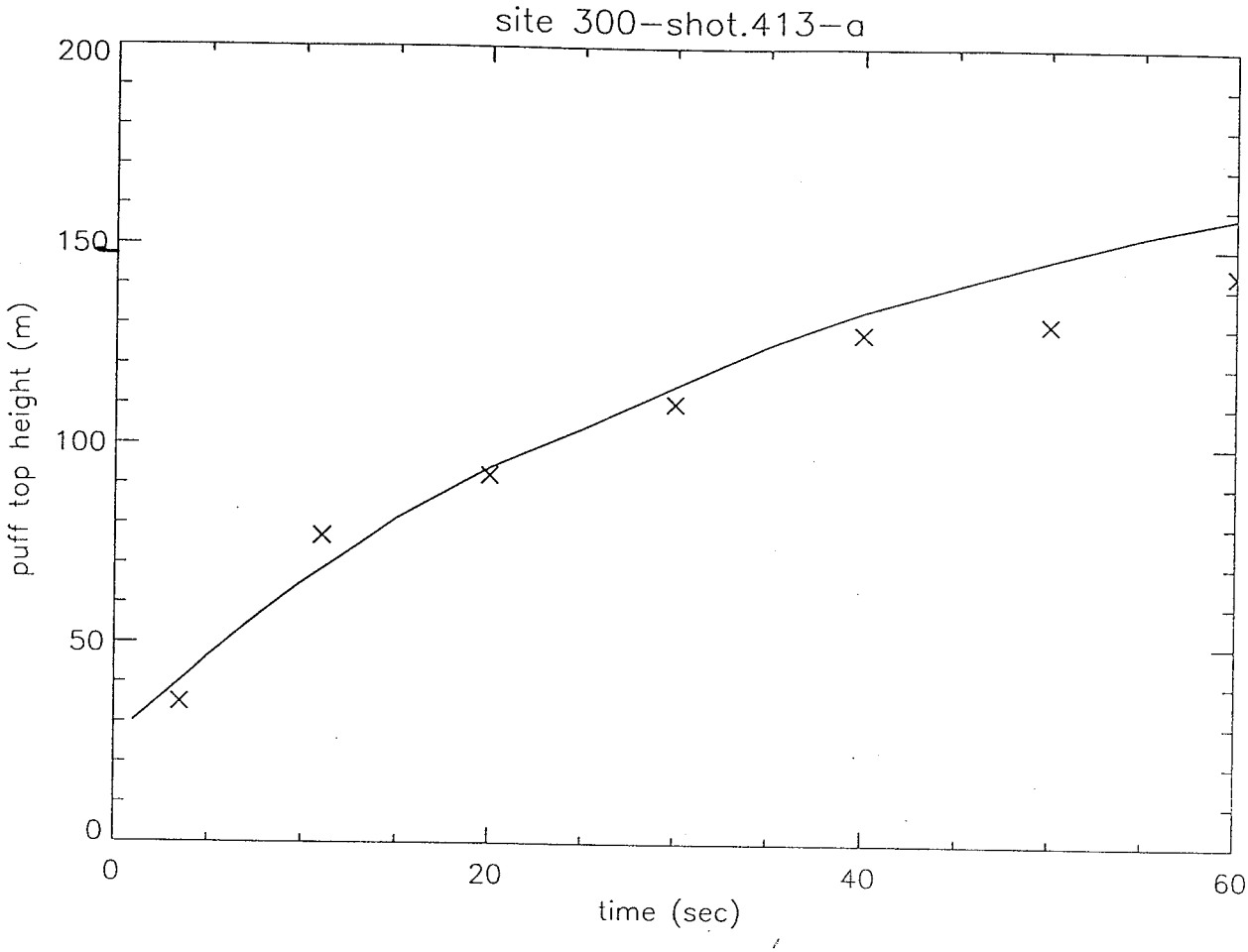

Figure 20. Height history for the LLNL Site 300 experiment, 413-a.

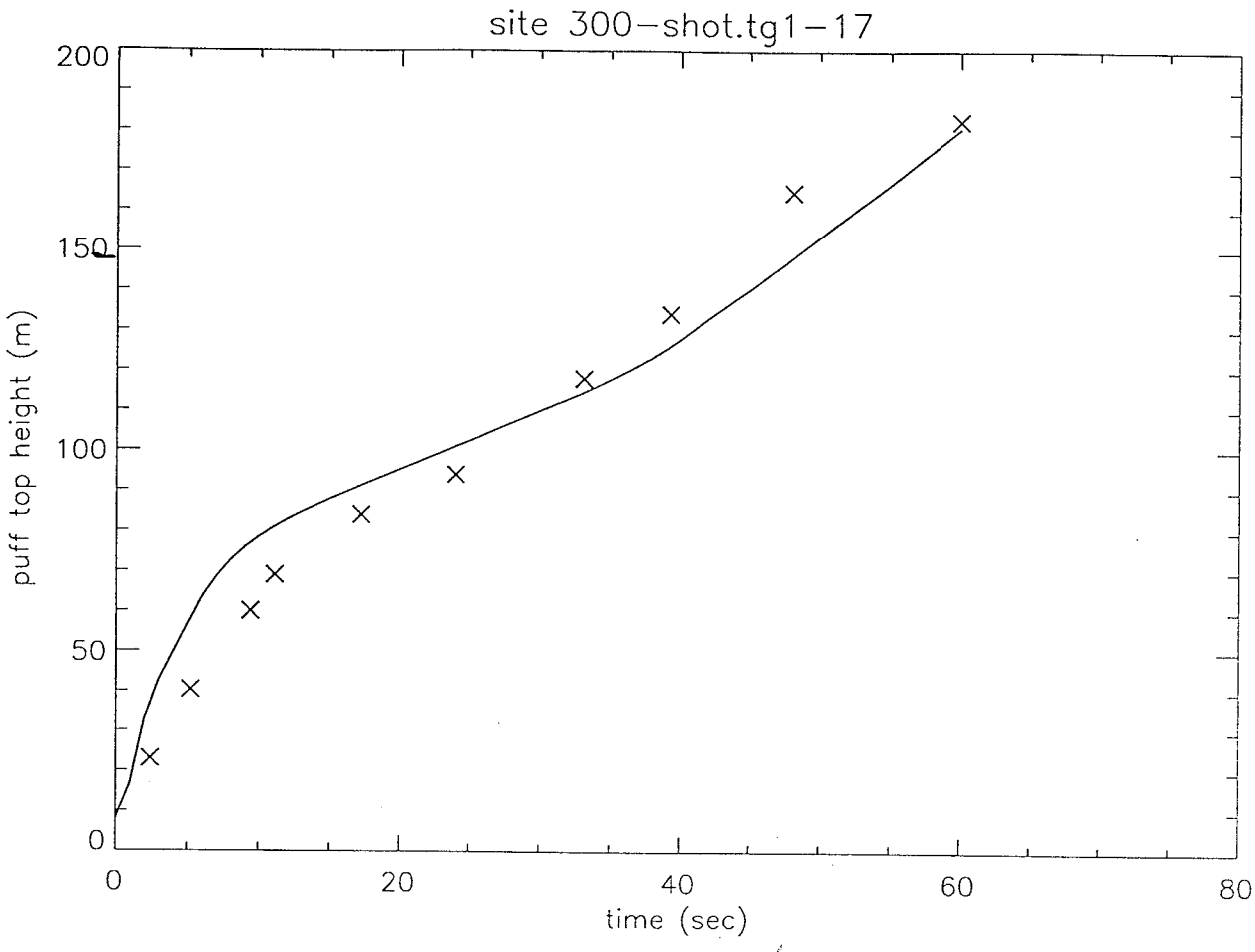

Figure 21. Height history for the LLNL Site 300 experiment, TG1-17.

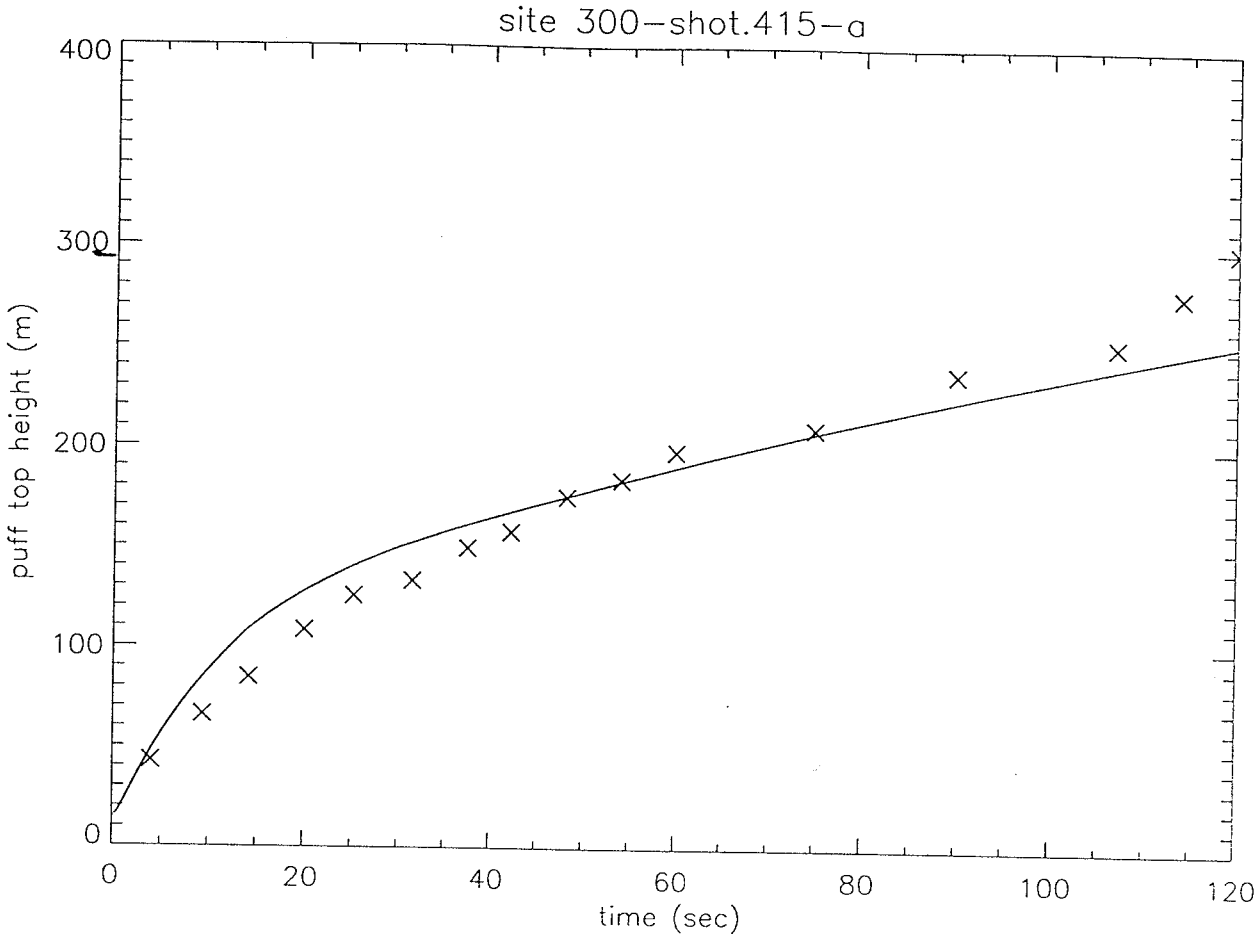

Figure 22. Height history for the LLNL Site 300 experiment, 415-a.

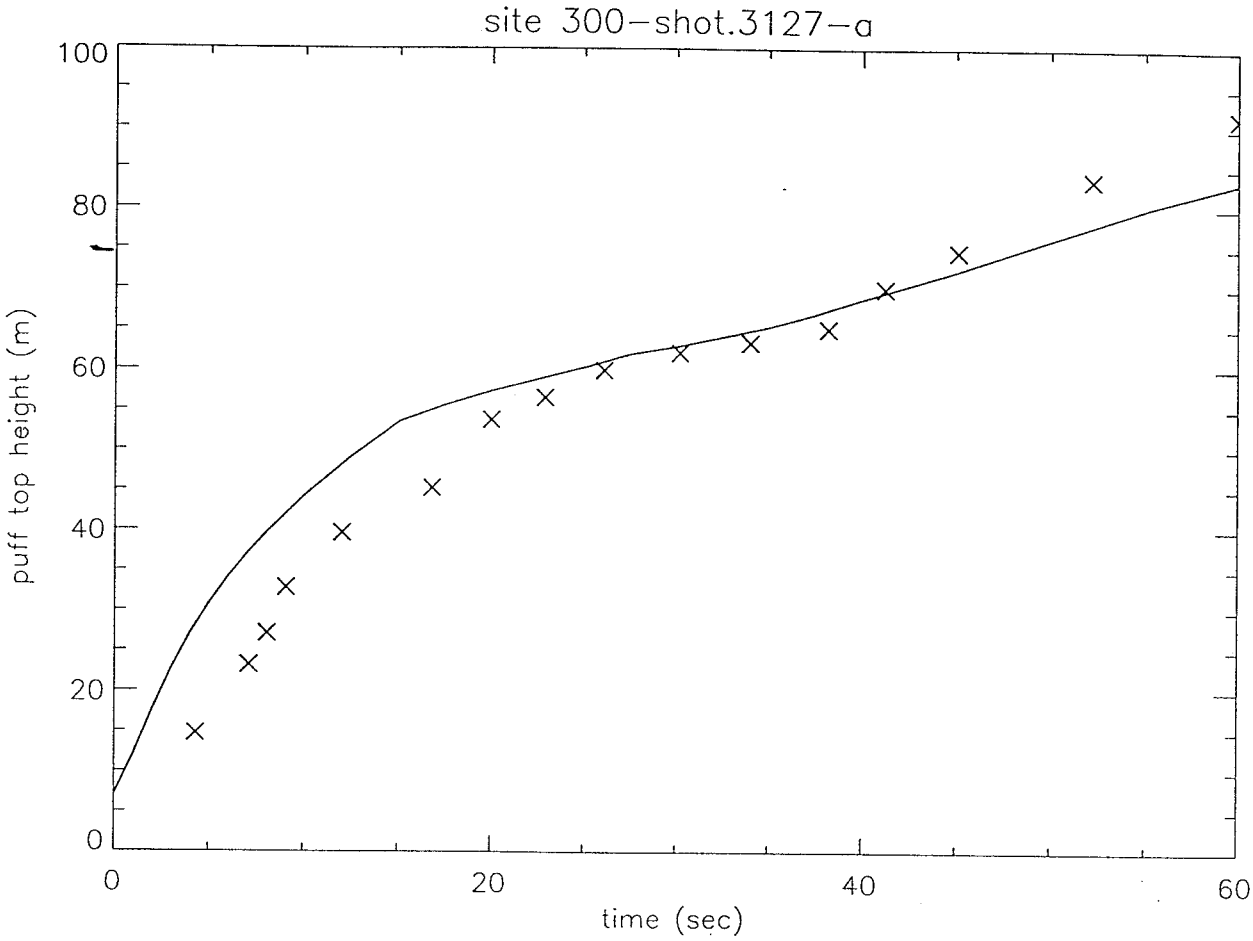

Figure 23. Height history for the LLNL Site 300 experiment, 3127-a.

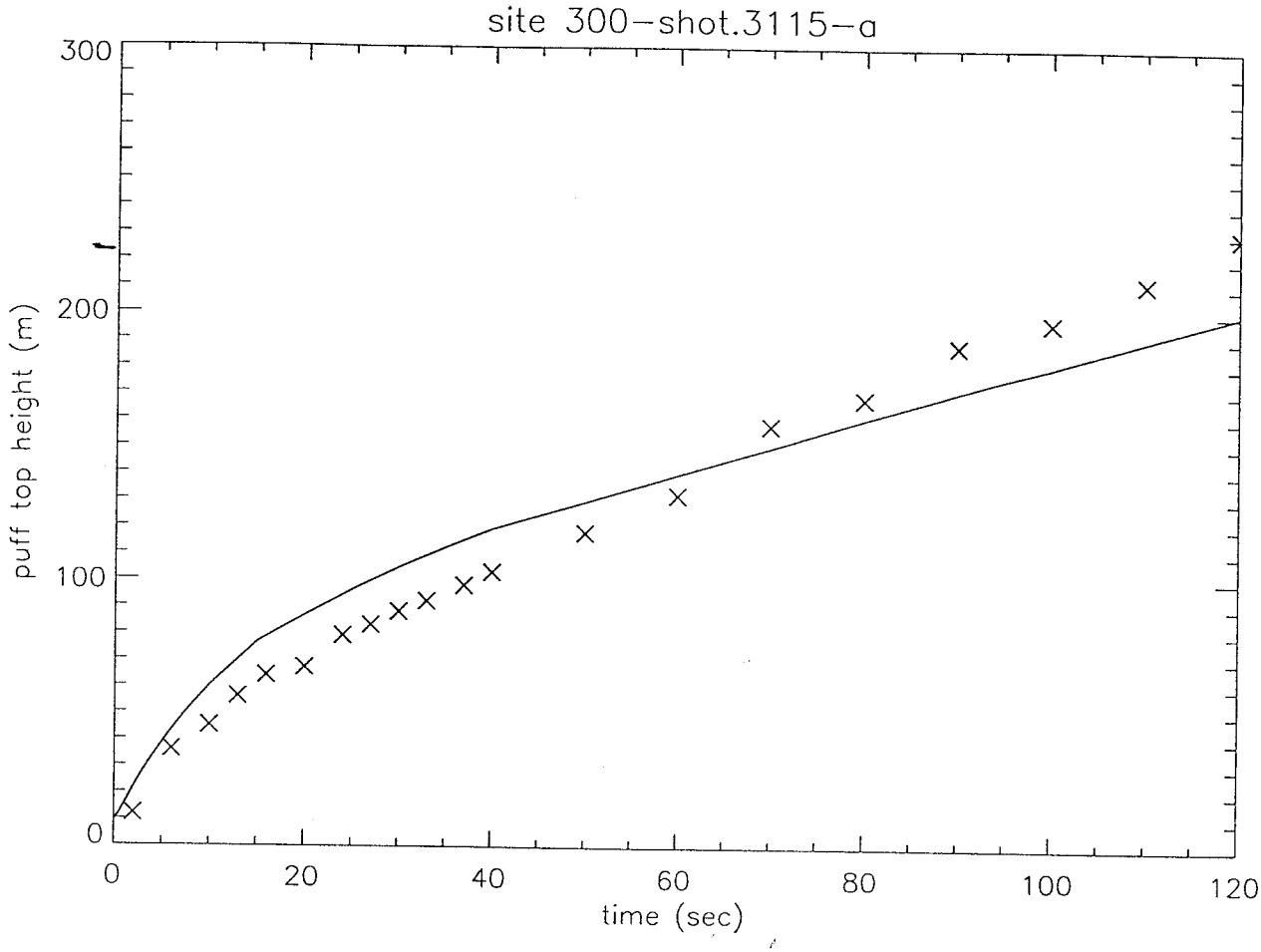

Figure 24. Height history for the LLNL Site 300 experiment, 3115-a

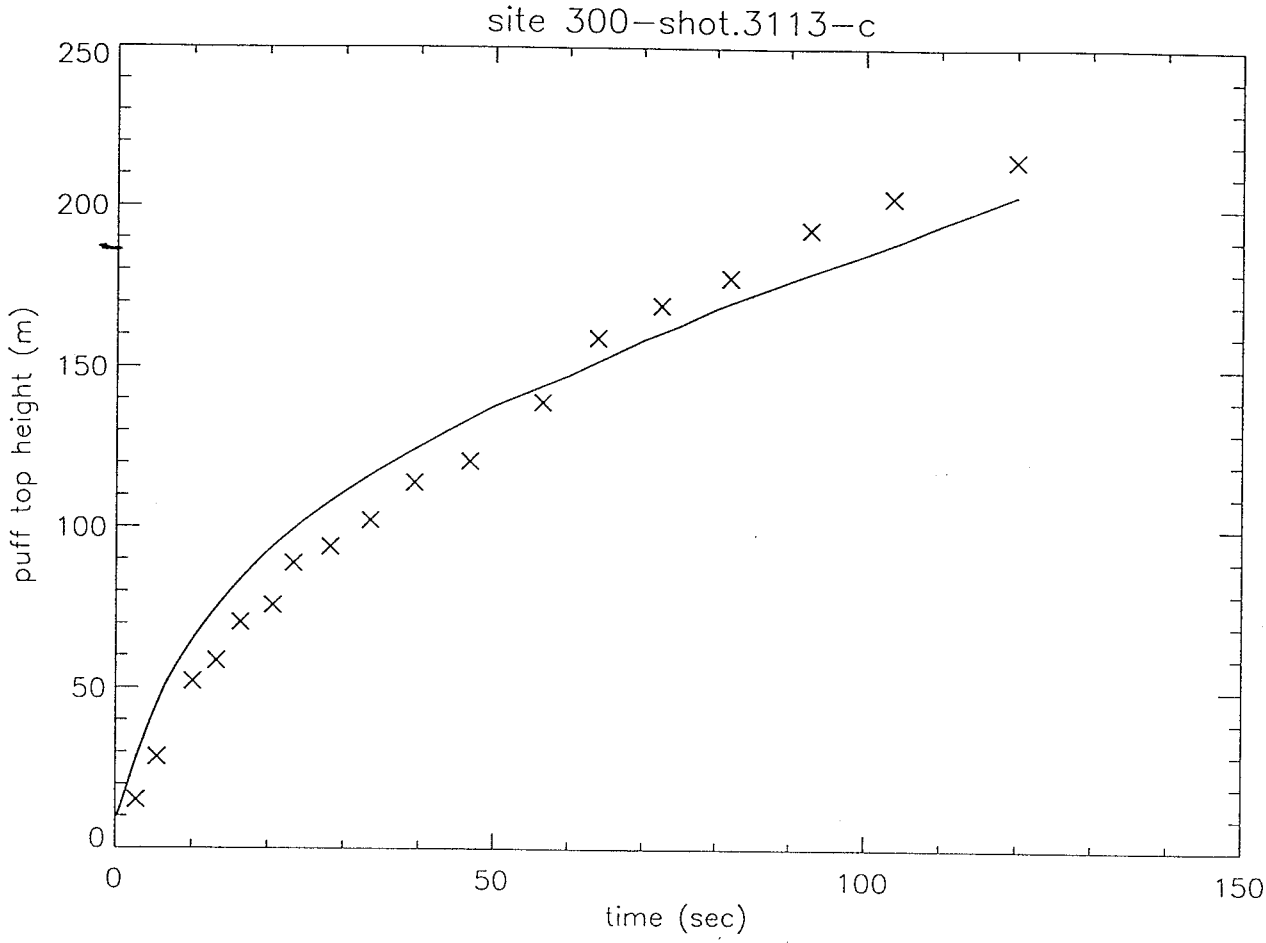

Figure 25. Height history for the LLNL Site 300 experiment, 3113-c.

Technical Information Department • **Lawrence Livermore National Laboratory**
University of California • Livermore, California 94551